SIAM J. NUMER. ANAL.
Vol. 58, No. 1, pp. 492–518

A ROBUST A POSTERIORI ERROR ESTIMATOR FOR DIVERGENCE-CONFORMING DISCONTINUOUS GALERKIN METHODS FOR THE OSEEN EQUATION*

ARBAZ KHAN† AND GUIDO KANSCHAT‡

Abstract. In this paper, a robust a posteriori error estimator for divergence-conforming discontinuous Galerkin methods for the Oseen equation is presented. Upper and local lower bounds for the velocity-pressure error in terms of the energy norm and a seminorm associated with the convective term are derived. We prove that the ratio of upper and lower bounds is independent of the Reynolds number. Thus the proposed estimator is fully robust. Specific numerical experiments are discussed to validate the theoretical results.

Key words. a posteriori error estimates, divergence-conforming DG methods, Oseen equations

AMS subject classification. 65M70

DOI. 10.1137/18M1169072

1. Introduction.

In addition to exhibiting corner singularities in elliptic partial differential equations, advection dominated problems also exhibit layers of rapid change at the boundary and in the interior. In order to obtain efficient numerical approximations, it is mandatory to use mesh adaptation for these layers. In this paper, we present an a posteriori error estimator in order to control adaptive mesh refinement for this purpose. In particular, we focus on deriving estimators which are efficient and robust in the sense that the ratio of upper and lower bounds is uniformly bounded with respect to the Reynolds number of the problem and the mesh size.

The main ingredients of adaptive finite element methods are *a posteriori* error estimators, which give information on the local error distribution. In particular, the reliable estimator controls the true error. Moreover, the reliable estimate can be used as a stopping criterion with an adaptive refinement process, while the efficiency of the error estimator ensures that the convergence rate of the error estimator is the same as the convergence rate of the true error. In the literature, most of the results based on error estimation for finite element methods (see [1, 22] and references therein) are restricted to pure diffusion problems. There are far fewer results on efficient and reliable a posteriori error estimators for advection-diffusion problems. In particular, robust a posteriori error estimators have upper and lower bounds for the error (measured in a suitable norm), which differ by a factor that is independent of the Péclet number of the advection-diffusion problem. In [21], Verfürth presented robust a posteriori error estimates for stationary advection-diffusion equations, which he extended to the time-dependent case in [20]. His key to efficient a posteriori error analysis is the use of an energy norm involving a dual norm of the directional derivative. Applying the same principle to discontinuous Galerkin (DG) methods,

*Received by the editors February 5, 2018; accepted for publication (in revised form) October 7, 2019; published electronically February 6, 2020.
https://doi.org/10.1137/18M1169072
Funding: The work of the authors was supported by the Mathematics Center Heidelberg (Match), University of Heidelberg, Germany, and by EPSRC grant EP/P013317.
†Corresponding author. Department of Mathematics, University of Manchester, Manchester, M13 9PL, UK (arbazkha@gmail.com).
‡Interdisziplinäres Zentrum für Wissenschaftliches Rechnen (IWR), Ruprecht-Karls-Universität Heidelberg, 69120 Heidelberg, Germany (kanschat@uni-heidelberg.de).

Schötzau and Zhu proposed a robust a posteriori error estimator for discontinuous Galerkin methods for advection-diffusion equations in [17]. Establishing robustness in the error estimation process is fundamentally important when solving flow problems with high Reynolds number. This is one of the major motivations for the development of a robust a posteriori error estimator for the Oseen equation.

Cockburn, Kanschat, and Schötzau presented the divergence-conforming discontinuous Galerkin method in [7, 6, 5]. In particular, divergence-conforming discontinuous Galerkin methods for incompressible Navier–Stokes problems are discussed in [7]. They used divergence-conforming finite element spaces for the approximation of the velocity (such as Brezzi–Douglas–Marini (BDM) or Raviart–Thomas (RT) spaces) and matching discontinuous spaces for the approximation of the pressure. Kanschat and Schötzau [14] proposed energy norm a posteriori error estimation for divergence-free discontinuous Galerkin approximations of the Navier–Stokes equations. A priori analysis for the DG method of the Oseen equation is discussed in [5].

In [22], Verfürth observed "a large ratio of the error estimators to the energy norm of the error" if the idea of standard error estimators for the self-adjoint elliptic problem is used. This is not surprising, since the residual is quite different in the advection dominated case. In this paper, we introduce a robust a posteriori error estimator for divergence-conforming DG finite elements (H^{div}-DG) for the Oseen problems. Upper and local lower bounds for the velocity-pressure error in terms of the energy norm and a seminorm associated with the advective term in the equation are derived. We show that the constants in the upper and lower bounds are independent of the Reynolds number and the mesh size. This ensures the robustness of the estimator. In our analysis, the error is decomposed into two parts: the conforming term and the remainder term. We use the standard technique (for more details, see also [10, 14, 17]) to deal with the conforming part and the stabilizing jump terms to control the remainder terms. We prove the main stability result that is key to our a posteriori error analysis. The rigorous proofs of reliability and efficiency theorems are discussed. To the best of our knowledge, the proposed error estimation analysis in this paper is the first comprehensive study of divergence-conforming DG finite elements for the Oseen problems.

The rest of the paper is organized as follows. In section 2, we introduce the divergence-conforming DG method for the Oseen equation. Section 3 is devoted to defining a robust a posteriori error estimator and presents reliability and efficiency estimates. Proofs of the reliability and efficiency theorems are given in section 4. In section 5, specific numerical experiments are discussed to validate the theoretical results.

2. H^{div}-DGFEM (DG finite element method) for the Oseen equation.

2.1. Function spaces. Let Ω be the bounded Lipschitz polygon in $\mathbb{R}^2$ with the boundary $\Gamma = \partial\Omega$. Given a bounded set $\omega \subset \Omega$, let $H^s(\omega)$ denote the standard Sobolev spaces with associated norm $||\cdot||_{s,\omega}$ for $s \geq 0$. In the case when $\omega = \Omega$, we use $||\cdot||_s$ instead of $||\cdot||_{s,\Omega}$. For $s = 0$, we set $L^2(\Omega) = H^0(\Omega)$. Let $\boldsymbol{H}^s(\omega) = [H^s(\omega)]^2$ denote the Sobolev spaces over the set of 2-dimensional vectors. The space of bounded functions on Ω is denoted by $L^\infty(\Omega)$. For $\boldsymbol{u} = (u_1, u_2)^t \in \mathbb{R}^2$ and $\boldsymbol{v} = (v_1, v_2)^t \in \mathbb{R}^2$, we define

$$\nabla \boldsymbol{v} = \begin{pmatrix} \frac{\partial v_1}{\partial x} & \frac{\partial v_1}{\partial y} \\ \frac{\partial v_2}{\partial x} & \frac{\partial v_2}{\partial y} \end{pmatrix}, \qquad \nabla \cdot \boldsymbol{v} = \frac{\partial v_1}{\partial x} + \frac{\partial v_2}{\partial y}, \qquad \boldsymbol{u} \otimes \boldsymbol{v} = \begin{pmatrix} u_1 v_1 & u_1 v_2 \\ u_2 v_1 & u_2 v_2 \end{pmatrix}.$$

Next, we introduce $L^2_0(\Omega), \boldsymbol{H}^{\mathrm{div}}(\Omega), \boldsymbol{H}^{\mathrm{div}}_0(\Omega)$, $\boldsymbol{H}^1_0(\Omega)$, and $W^{1,\infty}(\Omega)$ as follows:

$$
\begin{aligned}
L^2_0(\Omega) &:= \left\{ v \in L^2(\Omega) \;\middle|\; \int_\Omega v\, dx = 0 \right\},\\
\boldsymbol{H}^{\mathrm{div}}(\Omega) &:= \{\boldsymbol{v} \in \boldsymbol{L}^2(\Omega) = (L^2(\Omega))^2 \mid \nabla\cdot\boldsymbol{v} \in L^2(\Omega)\},\\
\boldsymbol{H}^{\mathrm{div}}_0(\Omega) &:= \{\boldsymbol{v} \in \boldsymbol{H}^{\mathrm{div}}(\Omega) \mid \boldsymbol{v}\cdot\boldsymbol{n} = 0 \ \text{ on } \ \partial\Omega\},\\
\boldsymbol{H}^1_0(\Omega) &:= \{\boldsymbol{v} \in \boldsymbol{H}^1(\Omega) \mid \boldsymbol{v}|_\Gamma = \boldsymbol{0}\},\\
W^{1,\infty}(\Omega) &:= \{v \in L^\infty(\Omega) \mid \nabla v \in L^\infty(\Omega)\}.
\end{aligned}
$$

2.2. Model problem. Consider the Oseen problem

$$
\begin{aligned}
-\nu\Delta\boldsymbol{u} + \underline{\boldsymbol{a}}\cdot\nabla\boldsymbol{u} + \nabla p + b\boldsymbol{u} &= \boldsymbol{f} \quad \text{in} \quad \Omega,\\
\nabla\cdot\boldsymbol{u} &= 0 \quad \text{in} \quad \Omega,\\
\boldsymbol{u} &= \boldsymbol{0} \quad \text{on} \quad \Gamma,
\end{aligned}
\tag{2.1}
$$

where $\boldsymbol{u}$, p, $\boldsymbol{f}$, ν, $\underline{\boldsymbol{a}}$, and b are the velocity, the pressure, a prescribed external body force, the kinematic viscosity, a convective velocity field, and a given scalar function, respectively. The force function $\boldsymbol{f}$, a viscosity coefficient ν, a convective velocity field $\underline{\boldsymbol{a}}$, and a given scalar function b satisfy the following conditions:

$$
\boldsymbol{f} \in \boldsymbol{L}^2(\Omega), \quad 0 < \nu \ll 1, \quad \underline{\boldsymbol{a}} \in W^{1,\infty}(\Omega), \quad \text{and} \quad b \in L^\infty(\Omega).
$$

Without loss of generality, we may make the assumption that the convective velocity field $\underline{\boldsymbol{a}}$ and size of Ω are of order one. Then ν^{-1} represents the Reynolds number of the problem. Our long-term goal is studying a robust a posteriori error estimator for divergence-conforming DG methods for both the transient and the stationary incompressible Navier–Stokes equations. Hence, we first study the Oseen equations, which appear by linearization of the incompressible Navier–Stokes equations using Picard's iterative scheme. In the first case, we assume that $\boldsymbol{u}$ is the velocity at the current time, $\underline{\boldsymbol{a}}$ is the velocity at the previous time step, and $b = 1/\Delta t$, which implies $b > 0$. In the second case, we have $b = 0$ for the steady-state Navier–Stokes problem. Thus we cannot assume $b > 0$. For the study of both cases, we assume that

$$
-\frac{1}{2}\nabla\cdot\underline{\boldsymbol{a}}(\boldsymbol{x}) + b(\boldsymbol{x}) \geq \beta, \quad \boldsymbol{x} \in \Omega,
\tag{2.2}
$$

for a constant $\beta \geq 0$. At the same time, there exists a constant $c_\star \geq 0$ such that

$$
|| - \nabla\cdot\underline{\boldsymbol{a}}(\boldsymbol{x}) + b(\boldsymbol{x})||_{L^\infty(\Omega)} \leq c_\star\beta.
$$

From [4, 9], we get the existence and uniqueness of a solution $(\boldsymbol{u}, p) \in \boldsymbol{H}^1_0(\Omega) \times L^2_0(\Omega)$ due to the condition (2.2).

2.3. Meshes, finite element spaces, and traces. First, we divide the domain Ω by a subdivision $\mathcal{T}_h$ into a mesh of shape-regular rectangular cells K. Let h_K, $\mathcal{E}^i(\mathcal{T}_h)$, $\mathcal{E}^\partial(\mathcal{T}_h)$, and $\mathcal{E}(\mathcal{T}_h)$ denote the diameter of an element K, the set of all interior edges of $\mathcal{T}_h$, the set of all boundary edges of $\mathcal{T}_h$, and the set of all edges of $\mathcal{T}_h$, respectively. Here, we restrict our attention to one-irregularly refined meshes $\mathcal{T}_h$, in which each elemental edge $E \in \mathcal{E}(\mathcal{T}_h)$ may contain at most one hanging node that can occur in the middle of it. For a given mesh $\mathcal{T}_h$, the broken spaces for the continuous and differentiable function spaces are denoted as $\mathcal{C}(\mathcal{T}_h)$ and $H^s(\mathcal{T}_h)$

which are the subspaces of $L^2(\Omega)$ such that the restriction to each mesh cell $K \in \mathcal{T}_h$ is in $\mathcal{C}(K)$ and $H^s(K)$, respectively. Now, we define $Q_k(K)$ and $Q_k(K)^d$ as the spaces of scalar and vector valued polynomials on K of degree at most integer $k > 0$. $RT_k(K) := \mathcal{P}_{k+1,k}(K) \times \mathcal{P}_{k,k+1}(K)$ denotes the RT space of degree $k > 0$. Here, $\mathcal{P}_{r,s}(K)$ is the space of the polynomial functions on K of degree at most integer $r > 0$ in x and at most integer $s > 0$ in y for $(x, y) \in K$; see [4, 6] for more details.

Remark 2.1. The inf-sup stability of discretizations with hanging nodes using RT elements is in part still an open question. In [16], there exists a stability proof only for the pair RT_k/Q_k defined in (2.3) and (2.4) with $k \geq 2$ for quadrilaterals with one-irregular meshes. However, we conjecture from our computational results that stability also holds for $k = 1$. Moreover, the stability result for the divergence-free elements proposed in [7] is not available for triangles with hanging nodes. On the other hand, locally refined triangular meshes without hanging nodes can be obtained using bisection. All of the results below are to be read in view of the restrictions cited in this remark.

Let K_1 and K_2 be mesh cells that have a common face $E \in \mathcal{E}(\mathcal{T}_h)$. The traces of function $u \in \mathcal{C}(\mathcal{T}_h)$ on E from K_1 and K_2 are defined as u_1 and u_2, respectively. Then the average operator $\{\{\cdot\}\}$ is as follows:

$$\{\{u\}\} = \frac{u_1 + u_2}{2}.$$

Let $\boldsymbol{n_1}$ and $\boldsymbol{n_2}$ be the outward unit normal vectors to K_1 and K_2, respectively. Then the jumps $[\![\cdot]\!]$ of these functions across E are defined as follows:

$$[\![u\boldsymbol{n}]\!] = u_1\boldsymbol{n}_1 + u_2\boldsymbol{n_2} = (u_1 - u_2)\boldsymbol{n}_1, \quad [\![u \otimes \boldsymbol{n}]\!] = u_1 \otimes \boldsymbol{n}_1 + u_2 \otimes \boldsymbol{n_2}, \quad [\![u]\!] = (u_1 - u_2).$$

Next, we define a unit tangential vector $\boldsymbol{t} = (-n_y, n_x)$ for a given unit normal vector $\boldsymbol{n} = (n_x, n_y)^T$. Thus $\boldsymbol{t}_2 = -\boldsymbol{t}_1$ for $\boldsymbol{n}_2 = -\boldsymbol{n}_1$.

Let Γ_{in} and Γ_{out} be the inflow and the outflow parts of Γ:

$$\Gamma_{\text{in}} = \{\boldsymbol{x} \in \Gamma : \underline{\boldsymbol{a}} \cdot \boldsymbol{n} < 0\}, \quad \Gamma_{\text{out}} = \{\boldsymbol{x} \in \Gamma : \underline{\boldsymbol{a}} \cdot \boldsymbol{n} \geq 0\}.$$

Similarly, we define the inflow and the outflow boundaries of an element K:

$$\partial K_{\text{in}} = \{\boldsymbol{x} \in \partial K : \underline{\boldsymbol{a}} \cdot \boldsymbol{n} < 0\}, \quad \partial K_{\text{out}} = \{\boldsymbol{x} \in \partial K : \underline{\boldsymbol{a}} \cdot \boldsymbol{n} \geq 0\}.$$

Let $\boldsymbol{V}_h$ be a discrete subspace of $\boldsymbol{H}_0^{\text{div}}(\Omega)$ such that

$$\boldsymbol{V}_h = \{v \in \boldsymbol{H}_0^{\text{div}} \mid \forall K \in \mathcal{T}_h : v|_K \in RT_k \quad \text{for } k \geq 1\} \tag{2.3}$$

and

$$\boldsymbol{V}_h^0 = \{v \in \boldsymbol{V}_h \mid \nabla \cdot v = 0\}.$$

Let Q_h be the discrete subspace of $L_0^2(\Omega)$ such that

$$Q_h = \{v \in L_0^2(\Omega) \mid \forall K \in \mathcal{T}_h : v|_K \in Q_k(K) \quad \text{for } k \geq 1\}. \tag{2.4}$$

The important property of the pair $\boldsymbol{V}_h \times Q_h$ is as follows: on the meshes considered,

$$\nabla \cdot \boldsymbol{V}_h \subset Q_h;$$

see [6] for more details.

We introduce the shorthand notation for integrals over meshes and sets of faces as

$$(f,g)_{\mathcal{T}_h} := \sum_{K\in\mathcal{T}_h} (f,g)_K; \quad \langle f,g\rangle_{\mathcal{E}(\mathcal{T}_h)} := \sum_{E\in\mathcal{E}(\mathcal{T}_h)} \langle f,g\rangle_E = \sum_{E\in\mathcal{E}(\mathcal{T}_h)} \int_E f\odot g\, ds,$$

where $\odot$ is a generic multiplication operator. Similarly, the seminorms are as follows:

$$||f||_{\mathcal{T}_h} := \sqrt{(f,f)_{\mathcal{T}_h}} \quad \text{and} \quad ||f||_{\mathcal{E}(\mathcal{T}_h)} := \sqrt{\langle f,f\rangle_{\mathcal{E}(\mathcal{T}_h)}}.$$

2.4. $\boldsymbol{H^{\mathrm{div}}}$-DG formulation for the Oseen problem. The discrete weak formulation of the problem (2.1) is as follows: find $(\boldsymbol{u},p)\in \boldsymbol{V}_h\times Q_h$ such that there holds

$$\mathcal{A}_h(\boldsymbol{u},p;\boldsymbol{v},q) = (\boldsymbol{f},\boldsymbol{v}) \quad \forall\ (\boldsymbol{v},q)\in \boldsymbol{V}_h\times Q_h, \tag{2.5}$$

where

$$\mathcal{A}_h(\boldsymbol{u},p;\boldsymbol{v},q) = a_h(\boldsymbol{u},\boldsymbol{v}) + o_h(\boldsymbol{u},\boldsymbol{v}) - (p,\nabla\cdot\boldsymbol{v}) - (q,\nabla\cdot\boldsymbol{u})$$

with

$$a_h(\boldsymbol{u},\boldsymbol{v}) = \nu(\nabla\boldsymbol{u},\nabla\boldsymbol{v})_{\mathcal{T}_h} + a_h^i(\boldsymbol{u},\boldsymbol{v}) + a_h^\partial(\boldsymbol{u},\boldsymbol{v}), \tag{2.6}$$

$$a_h^i(\boldsymbol{u},\boldsymbol{v}) = a_p^i(\boldsymbol{u},\boldsymbol{v}) - a_c^i(\boldsymbol{u},\boldsymbol{v}) - a_c^i(\boldsymbol{v},\boldsymbol{u}), \tag{2.7}$$

$$a_h^\partial(\boldsymbol{u},\boldsymbol{v}) = a_p^\partial(\boldsymbol{u},\boldsymbol{v}) - a_c^\partial(\boldsymbol{u},\boldsymbol{v}) - a_c^\partial(\boldsymbol{v},\boldsymbol{u}). \tag{2.8}$$

The interior face terms $a_p^i(\boldsymbol{u},\boldsymbol{v})$, $a_c^i(\boldsymbol{u},\boldsymbol{v})$ and the Nitsche terms are defined as

$$a_c^i(\boldsymbol{u},\boldsymbol{v}) = \langle\{\{\nu\nabla\boldsymbol{u}\}\},[\![\boldsymbol{v}\otimes\boldsymbol{n}]\!]\rangle_{\mathcal{E}^i(\mathcal{T}_h)}, \quad a_p^i(\boldsymbol{u},\boldsymbol{v}) = \langle\gamma_h^2[\![\boldsymbol{u}\otimes\boldsymbol{n}]\!],[\![\boldsymbol{v}\otimes\boldsymbol{n}]\!]\rangle_{\mathcal{E}^i(\mathcal{T}_h)},$$
$$a_c^\partial(\boldsymbol{u},\boldsymbol{v}) = \langle\nu\nabla\boldsymbol{u},\boldsymbol{v}\otimes\boldsymbol{n}\rangle_{\mathcal{E}^\partial(\mathcal{T}_h)}, \qquad a_p^\partial(\boldsymbol{u},\boldsymbol{v}) = 2\langle\gamma_h^2\boldsymbol{u}\otimes\boldsymbol{n},\boldsymbol{v}\otimes\boldsymbol{n}\rangle_{\mathcal{E}^\partial(\mathcal{T}_h)},$$

where $\gamma_h^2 = \frac{\gamma\nu}{h_E}$. Here, h_E is a suitably defined mesh size on the edge E, and $\gamma>0$ is a penalty parameter which is chosen sufficiently large, independently of the mesh size and the viscosity coefficient ν to guarantee the stability of the DG formulation.

The above bilinear forms are the same as the divergence-conforming DG methods for the Stokes system. The following bilinear form distinguishes the Oseen equations from the Stokes equations:

$$o_h(\boldsymbol{u},\boldsymbol{v}) = \sum_{K\in\mathcal{T}_h}\int_K ((b-\nabla\cdot\underline{\boldsymbol{a}})\boldsymbol{u}\boldsymbol{v} - \boldsymbol{u}\underline{\boldsymbol{a}}^T : \nabla\boldsymbol{v})\,\mathrm{d}\boldsymbol{x}$$
$$+ \sum_{K\in\mathcal{T}_h}\int_{\partial K_{\mathrm{out}}\cap\Gamma_{\mathrm{out}}} (\underline{\boldsymbol{a}}\cdot\boldsymbol{n}_K)\boldsymbol{u}\cdot\boldsymbol{v}d\boldsymbol{s} + \sum_{K\in\mathcal{T}_h}\int_{\partial K_{\mathrm{out}}\setminus\Gamma} (\underline{\boldsymbol{a}}\cdot\boldsymbol{n}_K)\boldsymbol{u}\cdot(\boldsymbol{v}-\boldsymbol{v}^e)d\boldsymbol{s}.$$

Here, $\boldsymbol{v}^e$ defines the exterior trace of $\boldsymbol{v}$ taken over the face under consideration and set to zero on the boundary. Now, we introduce the norm

$$|||(\boldsymbol{u},p)|||^2 = |||\boldsymbol{u}|||^2 + \nu^{-1}||p||_{\mathcal{T}_h}^2, \tag{2.9}$$

where

$$|||\boldsymbol{u}|||^2 = \nu||\nabla\boldsymbol{u}||_{\mathcal{T}_h}^2 + a_p^i(\boldsymbol{u},\boldsymbol{u}) + a_p^\partial(\boldsymbol{u},\boldsymbol{u}) + \beta||\boldsymbol{u}||_{\mathcal{T}_h}^2.$$

Next, we define

$$|\boldsymbol{u}|_A^2 = |\boldsymbol{u}\underline{\boldsymbol{a}}^T|_\star^2 + \sum_{E\in\mathcal{E}(\mathcal{T}_h)} \left(\beta h_E + \frac{h_E}{\nu}\right) |||[\![\boldsymbol{u}]\!]||_{0,E}^2, \tag{2.10}$$

where

$$|\underline{q}|_\star = \sup_{\boldsymbol{v}\in\boldsymbol{H}_0^1(\Omega)\setminus\{0\}} \frac{\int_\Omega \underline{q} : \nabla \boldsymbol{v}\, \mathrm{d}\boldsymbol{x}}{|||\boldsymbol{v}|||}.$$

For the bound on the convective derivative, we use the seminorm $|\boldsymbol{u}\underline{\boldsymbol{a}}^T|_\star^2$ and $h_E\nu^{-1}$ $|||[\![\boldsymbol{u}]\!]||_{0,E}^2$. To bound the reaction term, the jump terms $\beta h_E|||[\![\boldsymbol{u}]\!]||_{0,E}^2$ are used.

Remark 2.2. In [17, 22], the dual norm $||\cdot||_*$ and the seminorm $|\cdot|_*$ are discussed for the scalar advection-diffusion equation. Here, we discuss the details of the seminorm for the Oseen equations. Using Helmholtz decomposition for each row, we have

$$\underline{q} =: \boldsymbol{u}\underline{\boldsymbol{a}}^T = \nabla\phi - \underline{q}_0,$$

where $\phi \in \boldsymbol{H}_0^1(\Omega)$ solves

$$\int_\Omega \nabla\phi : \nabla\boldsymbol{v}\, d\boldsymbol{x} = \int_\Omega \underline{q} : \nabla\boldsymbol{v}\, d\boldsymbol{x} \quad \forall \boldsymbol{v} \in \boldsymbol{H}_0^1(\Omega),$$

and $\underline{q}_0 = \underline{q} - \nabla\phi$ is divergence free in the sense that

$$\int_\Omega \underline{q}_0 : \nabla\boldsymbol{v} d\boldsymbol{x} = 0 \quad \forall \boldsymbol{v} \in \boldsymbol{H}_0^1(\Omega).$$

Moreover, we have $|\underline{q}|_\star = 0$ if and only if $\underline{q} = \underline{q}_0$. Furthermore, if we introduce the norm

$$||\phi||_\star = \sup_{\boldsymbol{v}\in\boldsymbol{H}_0^1(\Omega)\setminus\{0\}} \frac{\int_\Omega \nabla\phi : \nabla\boldsymbol{v} d\boldsymbol{x}}{|||\boldsymbol{v}|||},$$

then we have

$$|\underline{q}|_\star = ||\phi||_\star.$$

3. Robust a posteriori error estimates. First, we define the scaling factors ρ_K and ρ_E by

$$\rho_K = \min\{h_K\nu^{-\frac{1}{2}}, \beta^{-\frac{1}{2}}\}, \quad \rho_E = \min\{h_E\nu^{-\frac{1}{2}}, \beta^{-\frac{1}{2}}\}.$$

In the case when $\beta = 0$, we choose $\rho_K = h_k\nu^{-\frac{1}{2}}$ and $\rho_E = h_E\nu^{-\frac{1}{2}}$.

Let $\boldsymbol{f}_h$, $\boldsymbol{a}_h$, and b_h represent piecewise polynomial approximations of $\boldsymbol{f}$, $\boldsymbol{a}$, and b, possibly discontinuous across elemental edges.

DEFINITION 3.1. *For $(\boldsymbol{u}_h, p_h) \in \boldsymbol{V}_h \times Q_h$ and $K \in \mathcal{T}_h$, the local error indicator η_K is*

$$\eta_K^2 := \eta_{R_K}^2 + \eta_{E_K}^2 + \eta_{J_K}^2,$$

with the internal residual η_{R_K}*, the edge residual* η_{E_K}*, and the trace residual* η_{J_K} *given by*

$$\eta_{R_K}^2 = \rho_K^2 ||\boldsymbol{f}_h + \nu\Delta\boldsymbol{u}_h - \underline{\boldsymbol{a}}_h \cdot \nabla\boldsymbol{u}_h - \nabla p_h - b_h\boldsymbol{u}_h||_{0,K}^2,$$

$$\eta_{E_K}^2 = \frac{1}{2}\sum_{E\in\partial K\setminus\Gamma} \nu^{-\frac{1}{2}}\rho_E ||[\![(p_h\underline{I} - \nu\nabla\boldsymbol{u}_h)\cdot\boldsymbol{n}]\!]||_{0,E}^2,$$

$$\eta_{J_K}^2 = \frac{1}{2}\sum_{E\in\partial K\setminus\Gamma}\left(\frac{\gamma\nu}{h_E}+\beta h_E+\frac{h_E}{\nu}\right)||[\![\boldsymbol{u}_h\otimes\boldsymbol{n}]\!]||_{0,E}^2 + \sum_{E\in\partial K\cap\Gamma}\left(\frac{\gamma\nu}{h_E}+\beta h_E+\frac{h_E}{\nu}\right)||\boldsymbol{u}_h||_{0,E}^2,$$

where $\underline{I}$ *is the* 2×2 *identity matrix. For* $(\boldsymbol{u}_h, p_h)\in \boldsymbol{V}_h\times Q_h$ *and* $K\in\mathcal{T}_h$*, the data oscillation term is given by*

$$\boldsymbol{\Theta}_K^2 = \rho_K^2(||\boldsymbol{f}-\boldsymbol{f}_h||_{0,K}^2 + ||(\underline{\boldsymbol{a}}-\underline{\boldsymbol{a}}_h)\cdot\nabla\boldsymbol{u}_h||_{0,K}^2 + ||(b-b_h)\boldsymbol{u}_h||_{0,K}^2).$$

Finally, we define the global error estimator η *and the data oscillation error* Θ *by*

$$\eta = \Big(\sum_{K\in\mathcal{T}_h}\eta_K^2\Big)^{\frac{1}{2}} \quad \textit{and} \quad \boldsymbol{\Theta} = \Big(\sum_{K\in\mathcal{T}_h}\boldsymbol{\Theta}_K^2\Big)^{\frac{1}{2}}. \tag{3.1}$$

3.1. Reliability and efficiency. In order to keep the following notation simple, the symbols $\lesssim$ and $\gtrsim$ are used to denote the bounds which are valid up to positive constants independent of the local mesh size, the viscosity coefficient ν, and the parameter β. In the case when $\gamma\geq 1$, the constants will also be independent of γ (see Lemma 4.2).

THEOREM 3.2 (reliability estimate). *Let* $(\boldsymbol{u}, p)$ *be the solution of the Oseen equation* (2.1)*, and let* $(\boldsymbol{u}_h, p_h)\in \boldsymbol{V}_h\times Q_h$ *be its* $\boldsymbol{H}^{\mathrm{div}}$ *DG approximation obtained by* (2.5)*. Let* η *and* $\boldsymbol{\Theta}$ *be the error estimator and the data approximation term in* (3.1)*. Then we obtain the following a posteriori error bound:*

$$|||\boldsymbol{u}-\boldsymbol{u}_h||| + \nu^{-1/2}||p-p_h||_{\mathcal{T}_h} + |\boldsymbol{u}-\boldsymbol{u}_h|_A \lesssim \eta + \boldsymbol{\Theta}. \tag{3.2}$$

THEOREM 3.3 (efficiency estimate). *Let* $(\boldsymbol{u}, p)$ *be the solution of the Oseen equation* (2.1)*, and let* $(\boldsymbol{u}_h, p_h)\in \boldsymbol{V}_h\times Q_h$ *be its* $\boldsymbol{H}^{\mathrm{div}}$ *DG approximation obtained by* (2.5)*. Let* η *and* $\boldsymbol{\Theta}$ *be the error estimator and the data approximation term in* (3.1)*. Then we obtain the following a posteriori error bound:*

$$\eta \lesssim |||\boldsymbol{u}-\boldsymbol{u}_h||| + \nu^{-1/2}||p-p_h||_{\mathcal{T}_h} + |\boldsymbol{u}-\boldsymbol{u}_h|_A + \boldsymbol{\Theta}. \tag{3.3}$$

Remark 3.1. In Theorems 3.2 and 3.3, the reliability and efficiency constants are independent of the viscosity coefficient ν and the parameter β. Thus, this confirms that the ratio of upper and lower bounds is independent of the Reynolds number, up to a data approximation error. Hence the proposed estimator η is robust in the viscosity coefficient ν and the parameter β.

4. Proofs.

4.1. Auxiliary forms and their properties. In this subsection, we discuss the properties of the DG forms from [7, 14]. The DG form $a_h(\boldsymbol{u},\boldsymbol{v})$ is well defined for functions $\boldsymbol{u},\boldsymbol{v}\in \boldsymbol{H}_0^1(\Omega)\cap\boldsymbol{V}_h$ but not for functions $\boldsymbol{u},\boldsymbol{v}$ in $\boldsymbol{H}_0^1(\Omega)$. We can overcome this difficulty by using a suitable lifting operator; see [14] for more details. Now we discuss a different and new approach, where we split the DG form into several parts

and avoid the continuity estimation of the consistency and symmetrization terms completely. First, we define the following forms:

$$
\begin{aligned}
D_h(\boldsymbol{u},\boldsymbol{v}) &= \sum_{K\in\mathcal{T}_h}\int_K (\nu\nabla\boldsymbol{u}:\nabla\boldsymbol{v} + (b-\nabla\cdot\underline{\boldsymbol{a}})\boldsymbol{u}\boldsymbol{v})d\boldsymbol{x},\\
O_h(\boldsymbol{u},\boldsymbol{v}) &= -\sum_{K\in\mathcal{T}_h}\int_K \boldsymbol{u}\underline{\boldsymbol{a}}^T:\nabla\boldsymbol{v}d\boldsymbol{x} + \sum_{K\in\mathcal{T}_h}\int_{\partial K_{\mathrm{out}}\cap\Gamma_{\mathrm{out}}}(\underline{\boldsymbol{a}}\cdot\boldsymbol{n}_K)\boldsymbol{u}\cdot\boldsymbol{v}d\boldsymbol{s}\\
&\quad + \sum_{K\in\mathcal{T}_h}\int_{\partial K_{\mathrm{out}}\setminus\Gamma}(\underline{\boldsymbol{a}}\cdot\boldsymbol{n}_K)\boldsymbol{u}\cdot(\boldsymbol{v}-\boldsymbol{v}^e)d\boldsymbol{s},\\
\mathcal{K}_h(\boldsymbol{u},\boldsymbol{v}) &= -\sum_{E\in\mathcal{E}(\mathcal{T}_h)}\int_E \{\!\{\nu\nabla\boldsymbol{u}\}\!\}:[\![\boldsymbol{v}\otimes\boldsymbol{n}]\!]d\boldsymbol{s} - \sum_{E\in\mathcal{E}(\mathcal{T}_h)}\int_E \{\!\{\nu\nabla\boldsymbol{v}\}\!\}:[\![\boldsymbol{u}\otimes\boldsymbol{n}]\!]d\boldsymbol{s},\\
J_h(\boldsymbol{u},\boldsymbol{v}) &= \sum_{E\in\mathcal{E}(\mathcal{T}_h)}\frac{\nu\gamma}{h_E}\int_E [\![\boldsymbol{u}\otimes\boldsymbol{n}]\!]\cdot[\![\boldsymbol{v}\otimes\boldsymbol{n}]\!]d\boldsymbol{s},\\
B_h(\boldsymbol{u},p) &= -\sum_{K\in\mathcal{T}_h}\int_K \nabla\cdot\boldsymbol{u}\,p\,d\boldsymbol{x}.
\end{aligned}
$$

Choose $\tilde{A}_h(\boldsymbol{u},\boldsymbol{v})$ as

$$\tilde{A}_h(\boldsymbol{u},\boldsymbol{v}) = D_h(\boldsymbol{u},\boldsymbol{v}) + J_h(\boldsymbol{u},\boldsymbol{v}) + O_h(\boldsymbol{u},\boldsymbol{v}). \tag{4.1}$$

The auxiliary form $\tilde{A}_h(\boldsymbol{u},\boldsymbol{v})$ is well defined for all $\boldsymbol{u},\boldsymbol{v}\in\boldsymbol{V}(h) = \boldsymbol{V}_h + \boldsymbol{H}_0^1(\Omega)$. Moreover, it holds that

$$\mathcal{A}_h(\boldsymbol{u},p;\boldsymbol{v},q) = \tilde{A}_h(\boldsymbol{u},\boldsymbol{v}) + \mathcal{K}_h(\boldsymbol{u},\boldsymbol{v}) + B_h(\boldsymbol{v},p) + B_h(\boldsymbol{u},q). \tag{4.2}$$

4.1.1. Continuity properties of the auxiliary forms. In the next two lemmas, we show that the auxiliary forms are continuous.

LEMMA 4.1. *There hold*

$$
\begin{aligned}
&|D_h(\boldsymbol{u},\boldsymbol{v})| \lesssim |||\boldsymbol{u}|||\,|||\boldsymbol{v}|||, \quad \boldsymbol{u},\boldsymbol{v}\in\boldsymbol{V}(h),\\
&|J_h(\boldsymbol{u},\boldsymbol{v})| \lesssim |||\boldsymbol{u}|||\,|||\boldsymbol{v}|||, \quad \boldsymbol{u},\boldsymbol{v}\in\boldsymbol{V}(h),\\
&|O_h(\boldsymbol{u},\boldsymbol{v})| \lesssim |\boldsymbol{u}\underline{\boldsymbol{a}}^T|_\star\,|||\boldsymbol{v}|||, \quad \boldsymbol{u}\in\boldsymbol{V}(h),\ \boldsymbol{v}\in\boldsymbol{H}_0^1(\Omega),\\
&|\tilde{A}_h(\boldsymbol{u},\boldsymbol{v})| \lesssim |||\boldsymbol{u}|||\,|||\boldsymbol{v}|||, \quad \boldsymbol{u},\boldsymbol{v}\in\boldsymbol{V}(h),\\
&|B_h(\boldsymbol{u},p)| \lesssim |||\boldsymbol{u}|||\,\nu^{-1/2}||p||_{\mathcal{T}_h}, \quad \boldsymbol{u}\in\boldsymbol{V}(h),\ p\in L^2(\Omega).
\end{aligned}
$$

Proof. The first two bounds directly follow from the consequence of the Cauchy–Schwarz inequality. To prove the third bound, we use the definition of $|\boldsymbol{u}\underline{\boldsymbol{a}}^T|_\star$. The fourth bound follows to combine the first three bounds. The last bound directly follows from the consequence of the Cauchy–Schwarz inequality. ∎

LEMMA 4.2. *Let $\boldsymbol{u}\in\boldsymbol{V}_h$ and $\boldsymbol{v}\in\boldsymbol{H}_0^1(\Omega)\cap\boldsymbol{V}_h$; then it holds that*

$$\mathcal{K}_h(\boldsymbol{u},\boldsymbol{v}) \lesssim \gamma^{-1/2}\Big(\sum_{E\in\mathcal{E}(\mathcal{T}_h)}\int_E \frac{\nu\gamma}{h_E}||[\![\boldsymbol{u}\otimes\boldsymbol{n}]\!]||_{0,E}^2\Big)^{1/2}|||\boldsymbol{v}|||.$$

Proof. Since $\boldsymbol{v} \in \boldsymbol{H}_0^1(\Omega) \cap \boldsymbol{V}_h$, then it follows that

$$\mathcal{K}_h(\boldsymbol{u}, \boldsymbol{v}) = - \sum_{E \in \mathcal{E}(\mathcal{T}_h)} \int_E \{\{\nu \nabla \boldsymbol{v}\}\} : [\![\boldsymbol{u} \otimes \boldsymbol{n}]\!] ds.$$

Applying the Cauchy–Schwarz inequality implies

$$\mathcal{K}_h(\boldsymbol{u}, \boldsymbol{v}) \lesssim \gamma^{-1/2} \Big(\sum_{E \in \mathcal{E}(\mathcal{T}_h)} \int_E \nu h_E |\nabla \boldsymbol{v}|^2 d\boldsymbol{s} \Big)^{1/2} \Big(\sum_{E \in \mathcal{E}(\mathcal{T}_h)} \int_E \frac{\nu\gamma}{h_E} |[\![\boldsymbol{u} \otimes \boldsymbol{n}]\!]|^2 d\boldsymbol{s} \Big)^{1/2}.$$

Using the shape-regularity of the mesh and the inverse trace estimate

$$||\nabla \boldsymbol{v}||_{0,\partial K}^2 \lesssim h_K^{-1/2} ||\nabla \boldsymbol{v}||_{0,K}, \quad \boldsymbol{v} \in \boldsymbol{H}_0^1(\Omega) \cap \boldsymbol{V}_h,$$

it follows that

$$\mathcal{K}_h(\boldsymbol{u}, \boldsymbol{v}) \lesssim \gamma^{-1/2} \Big(\sum_{K \in \mathcal{T}_h} \nu ||\nabla \boldsymbol{v}||_{0,K}^2 \Big)^{1/2} \Big(\sum_{E \in \mathcal{E}(\mathcal{T}_h)} \int_E \frac{\nu\gamma}{h_E} |[\![\boldsymbol{u} \otimes \boldsymbol{n}]\!]|^2 d\boldsymbol{s} \Big)^{1/2}.$$

Note that, for $\gamma \geq 1$, the above estimate can be bounded independently of γ. ∎

4.1.2. Coercivity condition. In the next lemma, we show that the auxiliary form $\tilde{A}_h(\boldsymbol{u}, \boldsymbol{u})$ is coercive for any $\boldsymbol{u} \in \boldsymbol{H}_0^1(\Omega)$.

LEMMA 4.3. *For any $\boldsymbol{u} \in \boldsymbol{H}_0^1(\Omega)$, the following estimate holds:*

$$\tilde{A}_h(\boldsymbol{u}, \boldsymbol{u}) \geq |||\boldsymbol{u}|||^2. \tag{4.3}$$

Proof. By (4.1), we have

$$\begin{aligned} \tilde{A}_h(\boldsymbol{u}, \boldsymbol{u}) &= D_h(\boldsymbol{u}, \boldsymbol{u}) + J_h(\boldsymbol{u}, \boldsymbol{u}) + O_h(\boldsymbol{u}, \boldsymbol{u}) \quad \forall\, \boldsymbol{u} \in \boldsymbol{H}_0^1(\Omega), \\ &= D_h(\boldsymbol{u}, \boldsymbol{u}) + O_h(\boldsymbol{u}, \boldsymbol{u}) \quad \forall\, \boldsymbol{u} \in \boldsymbol{H}_0^1(\Omega). \end{aligned}$$

Using (2.2), it follows that

$$\tilde{A}_h(\boldsymbol{u}, \boldsymbol{u}) \geq |||\boldsymbol{u}|||^2 \quad \forall\, \boldsymbol{u} \in \boldsymbol{H}_0^1(\Omega).$$

This completes the proof. ∎

4.1.3. Inf-sup condition. In [21, 17], the scalar form of the following lemma is discussed for advection-diffusion problems.

LEMMA 4.4. *The estimate*

$$\inf_{\boldsymbol{u} \in \boldsymbol{H}_0^1(\Omega) \setminus \{0\}} \sup_{\boldsymbol{v} \in \boldsymbol{H}_0^1(\Omega) \setminus \{0\}} \frac{\tilde{A}_h(\boldsymbol{u}, \boldsymbol{v})}{(|||\boldsymbol{u}||| + |\boldsymbol{u}\underline{\boldsymbol{a}}^T|_\star)|||\boldsymbol{v}|||} \geq C$$

holds for a positive constant $C > 0$.

Proof. Assume that $\boldsymbol{u} \in \boldsymbol{H}_0^1(\Omega)$ and $\theta \in (0, 1)$. Then there exists a $\boldsymbol{v}_\theta \in \boldsymbol{H}_0^1(\Omega)$ such that

$$|||\boldsymbol{v}_\theta||| = 1, \quad O_h(\boldsymbol{u}, \boldsymbol{v}_\theta) = - \sum_{K \in \mathcal{T}_h} \int_K \boldsymbol{u}\underline{\boldsymbol{a}}^T : \nabla \boldsymbol{v}_\theta d\boldsymbol{x} \geq \theta |\boldsymbol{u}\underline{\boldsymbol{a}}^T|_\star. \tag{4.4}$$

Applying Lemma 4.1 and (4.4) in (4.1) implies

$$\begin{aligned}\tilde{A}_h(\boldsymbol{u},\boldsymbol{v}_\theta) &= D_h(\boldsymbol{u},\boldsymbol{v}_\theta) + J_h(\boldsymbol{u},\boldsymbol{v}_\theta) + O_h(\boldsymbol{u},\boldsymbol{v}_\theta)\\ &\geq \theta|\boldsymbol{u}\underline{\boldsymbol{a}}^T|_\star - C_a|||\boldsymbol{u}||| \; |||\boldsymbol{v}_\theta|||,\\ &= \theta|\boldsymbol{u}\underline{\boldsymbol{a}}^T|_\star - C_a|||\boldsymbol{u}|||,\end{aligned}$$

where C_a is a positive constant. Next, we define

$$\boldsymbol{w}_\theta = \boldsymbol{u} + \frac{|||\boldsymbol{u}|||}{1+C_a}\boldsymbol{v}_\theta.$$

Then it holds that

$$|||\boldsymbol{w}_\theta||| \leq \left(1 + \frac{1}{1+C_a}\right)|||\boldsymbol{u}|||.$$

By the coercivity result of Lemma 4.3, it follows that

$$\tilde{A}_h(\boldsymbol{u},\boldsymbol{u}) \geq |||\boldsymbol{u}|||^2 \quad \forall \boldsymbol{u} \in \boldsymbol{H}_0^1(\Omega).$$

Hence, we can conclude that

$$\begin{aligned}\sup_{\boldsymbol{v}\in\boldsymbol{H}_0^1(\Omega)\setminus\{0\}} \frac{\tilde{A}_h(\boldsymbol{u},\boldsymbol{v})}{|||\boldsymbol{v}|||} &\geq \frac{\tilde{A}_h(\boldsymbol{u},\boldsymbol{w}_\theta)}{|||\boldsymbol{w}_\theta|||}\\ &\geq \frac{|||\boldsymbol{u}|||^2 + (1+C_a)^{-1}|||\boldsymbol{u}|||(\theta|\boldsymbol{u}\underline{\boldsymbol{a}}^T|_\star - C_a|||\boldsymbol{u}|||)}{(1+\frac{1}{1+C_a})|||\boldsymbol{u}|||}\\ &= \frac{1}{2+C_a}(|||\boldsymbol{u}||| + \theta|\boldsymbol{u}\underline{\boldsymbol{a}}^T|_\star).\end{aligned}$$

Here, $\theta \in (0,1)$ and $\boldsymbol{u} \in \boldsymbol{H}_0^1(\Omega)$ are arbitrary. This completes the proof. ∎

4.1.4. Stability estimate. In the next lemma, we establish the main stability result that is key to our a posteriori error analysis.

LEMMA 4.5. *For any* $(\boldsymbol{u},p) \in \boldsymbol{H}_0^1(\Omega)\times L_0^2(\Omega)$, *there is* $(\boldsymbol{v},q) \in \boldsymbol{H}_0^1(\Omega)\times L_0^2(\Omega)$ *with* $|||(\boldsymbol{v},q)||| \leq 1$ *and*

$$\mathcal{A}_h(\boldsymbol{u},p;\boldsymbol{v},q) \gtrsim |||(\boldsymbol{u},p)||| + |\boldsymbol{u}\underline{\boldsymbol{a}}^T|_\star.$$

Proof. If $(\boldsymbol{u},p) \in \boldsymbol{H}_0^1(\Omega)\times L_0^2(\Omega)$, then it holds that

$$\mathcal{A}_h(\boldsymbol{u},p;\boldsymbol{u},-p) \geq |||\boldsymbol{u}|||^2. \tag{4.5}$$

By a consequence of the continuous inf-sup condition (see [4, 9, 14]), there exists a field $\boldsymbol{v}_1 \in \boldsymbol{H}_0^1(\Omega)$ such that

$$-(p,\nabla\cdot\boldsymbol{v}_1) \geq C_\Omega\nu^{-1}||p||_0^2, \quad \nu^{1/2}||\nabla\boldsymbol{v}_1||_0 \leq \nu^{-1/2}||p||_0, \tag{4.6}$$

where $C_\Omega > 0$ is a continuous inf-sup constant depending on Ω.

Using Lemma 4.1 and (4.6), we obtain

$$\begin{aligned}\mathcal{A}_h(\boldsymbol{u},p;\boldsymbol{v}_1,0) &= \tilde{A}_h(\boldsymbol{u},\boldsymbol{v}_1) + B_h(\boldsymbol{v}_1,p)\\ &\geq C_\Omega\nu^{-1}||p||_0^2 - C|||\boldsymbol{u}|||| \; |||\boldsymbol{v}_1|||\\ &\geq C_\Omega\nu^{-1}||p||_0^2 - C|||\boldsymbol{u}|||| \; \nu^{-1/2}||p||_\Omega\\ &\geq \left(C_\Omega - \frac{C\epsilon}{2}\right)\nu^{-1}||p||_0^2 - \frac{C}{2\epsilon}|||\boldsymbol{u}|||^2,\end{aligned} \tag{4.7}$$

where $C > 0$ and $\epsilon > 0$ are positive constants. From Lemma 4.4, there exists a $\boldsymbol{v}_2$ such that

$$\tilde{A}_h(\boldsymbol{u}, \boldsymbol{v}_2) \geq C_1(|||\boldsymbol{u}||| + |\boldsymbol{u}\underline{\boldsymbol{a}}^T|_\star)^2, \quad |||\boldsymbol{v}_2||| \leq C_2|||\boldsymbol{u}||| \leq C_2(|||\boldsymbol{u}||| + |\boldsymbol{u}\underline{\boldsymbol{a}}^T|_\star), \tag{4.8}$$

where $C_1 > 0$ and $C_2 > 0$ are positive constants. Thus, we have

$$\begin{aligned}
\mathcal{A}_h(\boldsymbol{u}, p; \boldsymbol{v}_2, 0) &= \tilde{A}_h(\boldsymbol{u}, \boldsymbol{v}_2) + B_h(\boldsymbol{v}_2, p) \\
&\geq C_1(|||\boldsymbol{u}||| + |\boldsymbol{u}\underline{\boldsymbol{a}}^T|_\star)^2 - C_3^{1/2}\nu^{-1/2}||p||_0|||\boldsymbol{v}_2||| \\
&\geq \left(C_1 - \frac{C_2C_3\epsilon_1}{2}\right)(|||\boldsymbol{u}||| + |\boldsymbol{u}\underline{\boldsymbol{a}}^T|_\star)^2 - \frac{C_2}{2\epsilon_1}\nu^{-1}||p||_0^2
\end{aligned} \tag{4.9}$$

for positive constants $C_3, \epsilon_1 > 0$.

Next, we introduce some parameters δ_1 and δ_2. Using (4.5), (4.7), and (4.9), we obtain

$$\begin{aligned}
\mathcal{A}_h(\boldsymbol{u}, p; \boldsymbol{u} + \delta_1\boldsymbol{v}_1 + \delta_2\boldsymbol{v}_2, -p) &= \mathcal{A}_h(\boldsymbol{u}, p; \boldsymbol{u}, -p) + \delta_1\mathcal{A}_h(\boldsymbol{u}, p; \boldsymbol{v}_1, 0) + \delta_2\mathcal{A}_h(\boldsymbol{u}, p; \boldsymbol{v}_2, 0) \\
&\geq |||\boldsymbol{u}|||^2 + \delta_1\left(\left(C_\Omega - \frac{C\epsilon}{2}\right)\nu^{-1}||p||_0^2 - \frac{C}{2\epsilon}|||\boldsymbol{u}|||^2\right) \\
&+ \delta_2\left(\left(C_1 - \frac{C_2C_3\epsilon_1}{2}\right)(|||\boldsymbol{u}||| + |\boldsymbol{u}\underline{\boldsymbol{a}}^T|_\star)^2 - \frac{C_2}{2\epsilon_1}\nu^{-1}||p||_0^2\right) \\
&\geq \left(1 - \frac{\delta_1 C}{2\epsilon}\right)|||\boldsymbol{u}|||^2 + \left(\delta_1\left(C_\Omega - \frac{C\epsilon}{2}\right) - \delta_2\frac{C_2}{2\epsilon_1}\right)\nu^{-1}||p||_0^2 \\
&+ \delta_1\left(C_1 - \frac{C_2C_3\epsilon_1}{2}\right)(|||\boldsymbol{u}||| + |\boldsymbol{u}\underline{\boldsymbol{a}}^T|_\star)^2.
\end{aligned}$$

Making the specific choices $\epsilon = \frac{C_\Omega}{C}$, $\epsilon_1 = \frac{C_1}{C_2C_3}$, $\delta_2 = \frac{\delta_1 C_1 C_\Omega}{2C_2^2C_3}$, and $\delta_1 = \frac{C_\Omega}{C^2}$ gives

$$\begin{aligned}
\mathcal{A}_h(\boldsymbol{u}, p; \boldsymbol{u} + \delta_1\boldsymbol{v}_1 + \delta_2\boldsymbol{v}_2, -p) &\geq \min\left\{\frac{1}{2}, \frac{C_\Omega^2}{C^2}, \frac{C_\Omega^2C_1^2}{4C^2C_3C_2^2}\right\}(|||(\boldsymbol{u}, p)|||^2 + |\boldsymbol{u}\underline{\boldsymbol{a}}^T|_\star^2) \\
&\gtrsim |||(\boldsymbol{u}, p)|||^2 + |\boldsymbol{u}\underline{\boldsymbol{a}}^T|_\star^2.
\end{aligned} \tag{4.10}$$

Finally, using the definition of $|||\cdot|||$, (4.6), and (4.8) implies

$$\begin{aligned}
|||(\boldsymbol{u} + \delta_1\boldsymbol{v}_1 + \delta_2\boldsymbol{v}_2, -p)|||^2 &= |||\boldsymbol{u} + \delta_1\boldsymbol{v}_1 + \delta_2\boldsymbol{v}_2|||^2 + \nu^{-1}||p||_0^2 \\
&\lesssim |||\boldsymbol{u}|||^2 + \delta_1^2|||\boldsymbol{v}_1|||^2 + \delta_2^2|||\boldsymbol{v}_2|||^2 + \nu^{-1}||p||_0^2 \\
&\lesssim |||\boldsymbol{u}|||^2 + \nu^{-1}||p||_0^2.
\end{aligned} \tag{4.11}$$

Combining (4.10) and (4.11) gives the desired result. ∎

4.2. Approximation operators. First, we define the discontinuous RT space $\widetilde{\boldsymbol{V}}_h = \{\boldsymbol{v} \in \boldsymbol{L}^2(\Omega) : \boldsymbol{v}|_K \in RT_k(K), K \in \mathcal{T}_h\}$. From [14], we can introduce the conforming space $\boldsymbol{V}_h^c = \widetilde{\boldsymbol{V}}_h \cap \boldsymbol{H}_0^1(\Omega)$. The orthogonal complement of $\boldsymbol{V}_h^c$ in $\widetilde{\boldsymbol{V}}_h$ with respect to the norm $|||\cdot|||$ is defined by $\boldsymbol{V}_h^\perp$, such that $\widetilde{\boldsymbol{V}}_h = \boldsymbol{V}_h^c \oplus \boldsymbol{V}_h^\perp$.

Next, we define an averaging based approximation operator $\mathscr{A}_h : \widetilde{\boldsymbol{V}}_h \to \boldsymbol{V}_h^c$. Then from Proposition 5.2 of [11] and Lemmas 5.3 and 5.4 of [23] (see also [12, 17, 14]), the following estimates hold.

LEMMA 4.6. *For any* $\boldsymbol{v} \in \widetilde{\boldsymbol{V}}_h$*, the following estimates hold:*

$$\sum_{K\in\mathcal{T}_h} ||\boldsymbol{v} - \mathscr{A}_h\boldsymbol{v}||_{0,K}^2 \lesssim \sum_{K\in\mathcal{E}(\mathcal{T}_h)} h_E \int_E |[\![\boldsymbol{v}]\!]|^2 ds,$$

$$\sum_{K\in\mathcal{T}_h} ||\nabla(\boldsymbol{v} - \mathscr{A}_h\boldsymbol{v})||_{0,K}^2 \lesssim \sum_{K\in\mathcal{E}(\mathcal{T}_h)} h_E^{-1} \int_E |[\![\boldsymbol{v}]\!]|^2 ds.$$

Next, we prove the following approximation results that are needed for Theorem 3.2.

LEMMA 4.7. *For any* $\boldsymbol{v} \in \boldsymbol{H}_0^1(\Omega)$*, the following estimates hold:*

$$\Big(\sum_{K\in\mathcal{T}_h} \rho_K^{-2} ||\boldsymbol{v} - \boldsymbol{I}_h\boldsymbol{v}||_{0,K}^2\Big)^{1/2} \lesssim |||\boldsymbol{v}|||,$$

$$\Big(\sum_{E\in\mathcal{E}(\mathcal{T}_h)} \nu^{1/2}\rho_E^{-1} ||\boldsymbol{v} - \boldsymbol{I}_h\boldsymbol{v}||_{0,E}^2\Big)^{1/2} \lesssim |||\boldsymbol{v}|||.$$

Here, $\boldsymbol{I}_h$ *is the standard Scott–Zhang interpolant (see* [9] *for more details).*

Proof. By (4.5) of [14], we have

$$\sum_{K\in\mathcal{T}_h} h_K^{-2} ||\boldsymbol{v} - \boldsymbol{I}_h\boldsymbol{v}||_{0,K}^2 \lesssim ||\nabla\boldsymbol{v}||_{0,\Omega}^2.$$

If $\rho_K = \min\{h_K\nu^{-\frac{1}{2}}, \beta^{-\frac{1}{2}}\} = h_K\nu^{-\frac{1}{2}}$ for some K, then it holds that

$$\rho_K^{-2} ||\boldsymbol{v} - \boldsymbol{I}_h\boldsymbol{v}||_{0,K}^2 = h_K^{-2}\nu ||\boldsymbol{v} - \boldsymbol{I}_h\boldsymbol{v}||_{0,K}^2 \lesssim \nu ||\nabla\boldsymbol{v}||_{0,\widetilde{K}}^2.$$

Here, $\widetilde{K} := \cup\{K' \in \mathcal{T}_h : K' \cap K \neq \phi\}$. If $\rho_K = \beta^{-1/2} > 0$ for some K, then the estimate directly follows from the definition of the DG norm. A summation over each cell K in $\mathcal{T}_h$ leads to the first estimate of the lemma.

To prove the second estimate, again from (4.6) of [14], it follows that

$$\sum_{E\in\mathcal{E}(\mathcal{T}_h)} h_E^{-1} ||\boldsymbol{v} - \boldsymbol{I}_h\boldsymbol{v}||_{0,E}^2 \lesssim ||\nabla\boldsymbol{v}||_{0,\Omega}^2.$$

Let E be one of the edges in $\mathcal{E}(\mathcal{T}_h)$. If $\rho_E = \min\{h_E\nu^{-\frac{1}{2}}, \beta^{-\frac{1}{2}}\} = h_E\nu^{-\frac{1}{2}}$, then

$$\nu^{1/2}\rho_E^{-1} ||\boldsymbol{v} - \boldsymbol{I}_h\boldsymbol{v}||_{0,E}^2 = \nu h_E^{-1} ||\boldsymbol{v} - \boldsymbol{I}_h\boldsymbol{v}||_{0,E}^2 \lesssim \nu ||\nabla\boldsymbol{v}||_{0,\widetilde{E}}^2.$$

Here, $\widetilde{E} := \cup\{K' \in \mathcal{T}_h : K' \cap E \neq \phi\}$. If $\rho_E = \beta^{-1/2} > 0$, then it holds that

$$\nu^{1/2}\rho_E^{-1} ||\boldsymbol{v} - \boldsymbol{I}_h\boldsymbol{v}||_{0,E}^2 = \nu^{1/2}\beta^{1/2} ||\boldsymbol{v} - \boldsymbol{I}_h\boldsymbol{v}||_{0,E}^2.$$

Applying the trace inequality gives

$$\begin{aligned}
\nu^{1/2}\rho_E^{-1} ||\boldsymbol{v} - \boldsymbol{I}_h\boldsymbol{v}||_{0,E}^2 &\lesssim \nu^{1/2}\beta^{1/2}h_K^{-1} ||\boldsymbol{v} - \boldsymbol{I}_h\boldsymbol{v}||_{0,\widetilde{E}}^2 \\
&\quad + \nu^{1/2}\beta^{1/2} ||\boldsymbol{v} - \boldsymbol{I}_h\boldsymbol{v}||_{0,\widetilde{E}} ||\nabla(\boldsymbol{v} - \boldsymbol{I}_h\boldsymbol{v})||_{0,\widetilde{E}} \\
&\lesssim (\nu ||\nabla(\boldsymbol{v} - \boldsymbol{I}_h\boldsymbol{v})||_{0,\widetilde{E}}^2 + \beta ||\boldsymbol{v} - \boldsymbol{I}_h\boldsymbol{v}||_{0,\widetilde{E}}^2) \\
&\lesssim \nu ||\nabla\boldsymbol{v}||_{0,\widetilde{E}}^2 + \beta ||\boldsymbol{v}||_{0,\widetilde{E}}^2.
\end{aligned}$$

A summation over each edge E in $\mathcal{E}(\mathcal{T}_h)$ implies the second estimate of the lemma. ∎

4.3. Proof of Theorem 3.2. First, we decompose the DG velocity approximation uniquely into

$$\boldsymbol{u}_h = \boldsymbol{u}_h^c + \boldsymbol{u}_h^r,$$

where $\boldsymbol{u}_h^c \in \boldsymbol{V}_h^c$ and $\boldsymbol{u}_h^r \in \boldsymbol{V}_h^\perp$. Note that $\boldsymbol{u}_h \in \boldsymbol{V}_h$ and $\boldsymbol{u}_h^c \in \boldsymbol{V}_h^c \subset \boldsymbol{V}_h$; then $\boldsymbol{u}_h^r = \boldsymbol{u}_h^c - \boldsymbol{u}_h \in \boldsymbol{V}_h$.

Using the triangle inequality, we can conclude that

$$|||\boldsymbol{u} - \boldsymbol{u}_h||| + |\boldsymbol{u} - \boldsymbol{u}_h|_A \le |||\boldsymbol{u} - \boldsymbol{u}_h^c||| + |\boldsymbol{u} - \boldsymbol{u}_h^c|_A + |||\boldsymbol{u}_h^r||| + |\boldsymbol{u}_h^r|_A. \tag{4.12}$$

In the next three lemmas, we show that the continuous error $\boldsymbol{u} - \boldsymbol{u}_h^c$, the remaining term $\boldsymbol{u}_h^r$, and the pressure error $p - p_h$ can be bounded by the global error estimator η and the data oscillation error Θ.

4.3.1. Upper bound for the remaining term $\boldsymbol{u}_h^r$. The upper bound for the remaining term $\boldsymbol{u}_h^r$ is proved in the following lemma.

LEMMA 4.8. *The estimate*

$$|||\boldsymbol{u}_h^r||| + |\boldsymbol{u}_h^r|_A \lesssim \eta \tag{4.13}$$

holds.

Proof. Using $[\![\boldsymbol{u}_h^r]\!] = [\![\boldsymbol{u}_h]\!]$, (2.9), and (2.10), we have

$$\begin{aligned}|||\boldsymbol{u}_h^r||| + |\boldsymbol{u}_h^r|_A = &\sum_{K\in\mathcal{T}_h} (\nu||\nabla \boldsymbol{u}_h^r||_{0,K}^2 + \beta||\boldsymbol{u}_h^r||_{0,K}^2) + |\boldsymbol{u}_h^r \underline{\boldsymbol{a}}^T|_*^2 \\ &+ \sum_{E\in\mathcal{E}(\mathcal{T}_h)} \left(\frac{\gamma\nu}{h_E} + \beta h_E + \frac{h_E}{\nu}\right) ||[\![\boldsymbol{u}_h]\!]||_{0,E}^2.\end{aligned}$$

By the definition of the trace residual η_{J_K}, it follows that

$$|||\boldsymbol{u}_h^r||| + |\boldsymbol{u}_h^r|_A \le \sum_{K\in\mathcal{T}_h} (\nu||\nabla \boldsymbol{u}_h^r||_{0,K}^2 + \beta||\boldsymbol{u}_h^r||_{0,K}^2) + |\boldsymbol{u}_h^r \underline{\boldsymbol{a}}^T|_*^2 + \sum_{K\in\mathcal{T}_h} \eta_{J_K}^2.$$

Thus, we need to establish the bound for the volume terms and for the term involving the $|\cdot|_\star$ seminorm. Using Lemma 4.6 and the definition of the trace residual η_{J_K} gives

$$\begin{aligned}\nu \sum_{K\in\mathcal{T}_h} ||\nabla \boldsymbol{u}_h^r||_{0,K}^2 &\lesssim \sum_{E\in\mathcal{E}(\mathcal{T}_h)} \frac{\nu}{h_E} ||[\![\boldsymbol{u}_h]\!]||_{0,E}^2 = \sum_{E\in\mathcal{E}(\mathcal{T}_h)} \frac{\nu\gamma}{h_E\gamma} ||[\![\boldsymbol{u}_h]\!]||_{0,E}^2 \lesssim \gamma^{-1} \sum_{K\in\mathcal{T}_h} \eta_{J_K}^2, \\ \sum_{K\in\mathcal{T}_h} \beta||\boldsymbol{u}_h^r||_{0,K}^2 &\lesssim \sum_{E\in\mathcal{E}(\mathcal{T}_h)} \beta h_E ||[\![\boldsymbol{u}_h]\!]||_{0,E}^2 \lesssim \sum_{K\in\mathcal{T}_h} \eta_{J_K}^2.\end{aligned}$$

To estimate the $|\boldsymbol{u}_h^r \underline{\boldsymbol{a}}^T|_\star$, we use the definition of the seminorm; then

$$|\boldsymbol{u}_h^r \underline{\boldsymbol{a}}^T|_*^2 = \sup_{\boldsymbol{v}\in\boldsymbol{H}_0^1(\Omega)\setminus\{0\}} \frac{(\int_\Omega \boldsymbol{u}_h^r \underline{\boldsymbol{a}}^T : \nabla \boldsymbol{v} d\boldsymbol{x})^2}{|||\boldsymbol{v}|||^2}.$$

Applying the Cauchy–Schwarz inequality yields

$$|\boldsymbol{u}_h^r \underline{\boldsymbol{a}}^T|_*^2 \lesssim \sup_{\boldsymbol{v}\in\boldsymbol{H}_0^1(\Omega)\setminus\{0\}} \frac{||\boldsymbol{u}_h^r||_{0,\Omega}^2 ||\nabla \boldsymbol{v}||_{0,\Omega}^2}{|||\boldsymbol{v}|||^2} = \sup_{\boldsymbol{v}\in\boldsymbol{H}_0^1(\Omega)\setminus\{0\}} \frac{||\boldsymbol{u}_h^r||_{0,\Omega}^2 \nu ||\nabla \boldsymbol{v}||_{0,\Omega}^2}{\nu|||\boldsymbol{v}|||^2}.$$

Again, using Lemma 4.6 and the definition of the trace residual η_{J_K}, it holds that

$$|\boldsymbol{u}_h^r \underline{\boldsymbol{a}}^T|_*^2 \lesssim \frac{1}{\nu}||\boldsymbol{u}_h^r||_{0,\Omega}^2 \lesssim \sum_{E\in\mathcal{E}(\mathcal{T}_h)} \frac{h_E}{\nu}||[\![\boldsymbol{u}_h]\!]||_{0,E}^2 \lesssim \sum_{K\in\mathcal{T}_h} \eta_{J_K}^2. \tag{4.14}$$

This completes the proof. ∎

4.3.2. Upper bound for the continuous error $\boldsymbol{u}-\boldsymbol{u}_h^c$ and for the pressure error $\boldsymbol{p}-\boldsymbol{p}_h$. In the next two lemmas, we prove the upper bound for the continuous error $\boldsymbol{u}-\boldsymbol{u}_h^c$ and for the pressure error $p-p_h$.

LEMMA 4.9. *The estimate*

$$\int_\Omega \boldsymbol{f}\cdot(\boldsymbol{v}-\boldsymbol{I}_h\boldsymbol{v})d\boldsymbol{x} - \tilde{A}_h(\boldsymbol{u}_h,\boldsymbol{v}-\boldsymbol{I}_h\boldsymbol{v}) - B_h(p_h,\boldsymbol{v}-\boldsymbol{I}_h\boldsymbol{v}) \lesssim (\eta+\boldsymbol{\Theta})|||\boldsymbol{v}||| \tag{4.15}$$

holds for any $\boldsymbol{v}\in\boldsymbol{H}_0^1(\Omega)$. Here, $\boldsymbol{I}_h$ is the interpolant discussed in Lemma 4.7.

Proof. Define

$$\boldsymbol{T} = \int_\Omega \boldsymbol{f}\cdot(\boldsymbol{v}-\boldsymbol{I}_h\boldsymbol{v})d\boldsymbol{x} - \tilde{A}_h(\boldsymbol{u}_h,\boldsymbol{v}-\boldsymbol{I}_h\boldsymbol{v}) - B_h(p_h,\boldsymbol{v}-\boldsymbol{I}_h\boldsymbol{v}).$$

Using integration by parts, we conclude that

$$\boldsymbol{T} = \boldsymbol{T}_1+\boldsymbol{T}_2+\boldsymbol{T}_3,$$

where

$$\begin{aligned}
\boldsymbol{T}_1 &= \sum_{K\in\mathcal{T}_h}\int_\Omega (\boldsymbol{f}+\nu\Delta\boldsymbol{u}_h - \underline{\boldsymbol{a}}\cdot\nabla\boldsymbol{u}_h - b\boldsymbol{u}_h - \nabla p_h)\cdot(\boldsymbol{v}-\boldsymbol{I}_h\boldsymbol{v})d\boldsymbol{x},\\
\boldsymbol{T}_2 &= \sum_{K\in\mathcal{T}_h}\int_{\partial K} ((p_h\underline{I}-\nu\nabla\boldsymbol{u}_h)\cdot\boldsymbol{n}_K)\cdot(\boldsymbol{v}-\boldsymbol{I}_h\boldsymbol{v})d\boldsymbol{s},\\
\boldsymbol{T}_3 &= \sum_{K\in\mathcal{T}_h}\int_{\partial K_{\mathrm{in}}\setminus\Gamma} \underline{\boldsymbol{a}}\cdot\boldsymbol{n}_K(\boldsymbol{u}_h-\boldsymbol{u}_h^e)\cdot(\boldsymbol{v}-\boldsymbol{I}_h\boldsymbol{v})d\boldsymbol{s}.
\end{aligned}$$

Now, we add and subtract the data approximation terms in $\boldsymbol{T}_1$. Then

$$\begin{aligned}
\boldsymbol{T}_1 = &\sum_{K\in\mathcal{T}_h}\int_\Omega (\boldsymbol{f}_h+\nu\Delta\boldsymbol{u}_h - \underline{\boldsymbol{a}}_h\cdot\nabla\boldsymbol{u}_h - b_h\boldsymbol{u}_h - \nabla p_h)\cdot(\boldsymbol{v}-\boldsymbol{I}_h\boldsymbol{v})d\boldsymbol{x}\\
&+\sum_{K\in\mathcal{T}_h}\int_\Omega ((\boldsymbol{f}-\boldsymbol{f}_h)-(\underline{\boldsymbol{a}}-\underline{\boldsymbol{a}}_h)\cdot\nabla\boldsymbol{u}_h-(b-b_h)\boldsymbol{u}_h)\cdot(\boldsymbol{v}-\boldsymbol{I}_h\boldsymbol{v})d\boldsymbol{x}.
\end{aligned}$$

Applying the Cauchy–Schwarz inequality and Lemma 4.7 implies

$$\begin{aligned}
\boldsymbol{T}_1 &\lesssim \Big(\sum_{K\in\mathcal{T}_h}\eta_{R_K}^2\Big)^{\frac12}\Big(\sum_{K\in\mathcal{T}_h}\rho_K^{-2}||\boldsymbol{v}-\boldsymbol{I}_h\boldsymbol{v}||_{0,K}^2\Big)^{\frac12} + \Big(\sum_{K\in\mathcal{T}_h}\boldsymbol{\Theta}_K^2\Big)^{\frac12}\Big(\sum_{K\in\mathcal{T}_h}\rho_K^{-2}||\boldsymbol{v}-\boldsymbol{I}_h\boldsymbol{v}||_{0,K}^2\Big)^{\frac12}\\
&\lesssim \Big(\sum_{K\in\mathcal{T}_h}(\eta_{R_K}^2+\boldsymbol{\Theta}_K^2)\Big)^{\frac12}|||\boldsymbol{v}|||.
\end{aligned}$$

Rewriting $\boldsymbol{T}_2$ in terms of a sum over interior edges, we get

$$\boldsymbol{T}_2 = \sum_{E\in\mathcal{E}^i(\mathcal{T}_h)} \int_E [\![p_h \underline{I} - \nu\nabla \boldsymbol{u}_h]\!] \cdot (\boldsymbol{v} - \boldsymbol{I}_h\boldsymbol{v}) ds.$$

Applying the Cauchy–Schwarz inequality and Lemma 4.7 implies

$$\begin{aligned}\boldsymbol{T}_2 &\lesssim \Big(\sum_{E\in\mathcal{E}^i(\mathcal{T}_h)} \nu^{-1/2}\rho_E ||[\![p_h\underline{I} - \nu\nabla\boldsymbol{u}_h]\!]||^2_{0,E} \Big)^{1/2} \Big(\sum_{E\in\mathcal{E}^i(\mathcal{T}_h)} \nu^{1/2}\rho_E^{-1} ||\boldsymbol{v} - \boldsymbol{I}_h\boldsymbol{v}||^2_{0,E} \Big)^{1/2} \\ &\lesssim \Big(\sum_{E\in\mathcal{E}^i(\mathcal{T}_h)} \eta^2_{E_K} \Big)^{1/2} |||\boldsymbol{v}|||.\end{aligned}$$

Using the Cauchy–Schwarz inequality and Lemma 4.7 in $\boldsymbol{T}_3$ gives

$$\boldsymbol{T}_3 \lesssim \Big(\sum_{E\in\mathcal{E}^i(\mathcal{T}_h)} \nu^{-1/2}\rho_E ||[\![\boldsymbol{u}_h]\!]||^2_{0,E} \Big)^{1/2} \Big(\sum_{E\in\mathcal{E}^i(\mathcal{T}_h)} \nu^{1/2}\rho_E^{-1} ||\boldsymbol{v} - \boldsymbol{I}_h\boldsymbol{v}||^2_{0,E} \Big)^{1/2}.$$

Since $\rho_E \le h_K\nu^{-1/2}$, we get

$$\boldsymbol{T}_3 \lesssim \Big(\sum_{K\in\mathcal{T}_h} \eta^2_{J_K} \Big)^{1/2} |||\boldsymbol{v}|||.$$

Combining the above estimates leads to the stated result. ∎

LEMMA 4.10. *The estimate*

$$||||\boldsymbol{u} - \boldsymbol{u}_h^c||| + |\boldsymbol{u} - \boldsymbol{u}_h^c|_A + \nu^{-1/2}||p - p_h||_{\mathcal{T}_h} \lesssim \eta + \boldsymbol{\Theta}$$

holds.

Proof. Since $|\boldsymbol{u} - \boldsymbol{u}_h^c|_A = |\boldsymbol{u} - \boldsymbol{u}_h^c|_*$ and $(\boldsymbol{u} - \boldsymbol{u}_h^c, p - p_h) \in \boldsymbol{H}^1_0(\Omega) \times L^2_0(\Omega)$, using Lemma 4.5 we have

$$|||\boldsymbol{u} - \boldsymbol{u}_h^c||| + |\boldsymbol{u} - \boldsymbol{u}_h^c|_* + \nu^{-1/2}||p - p_h||_{\mathcal{T}_h} \lesssim \mathcal{A}_h(\boldsymbol{u} - \boldsymbol{u}_h^c, p - p_h; \boldsymbol{v}, q) \tag{4.16}$$

for some $(\boldsymbol{v}, q) \in \boldsymbol{H}^1_0(\Omega) \times L^2_0(\Omega)$ with $|||(\boldsymbol{v}, q)||| \le 1$.

For any pair $(\boldsymbol{v}, q) \in \boldsymbol{H}^1_0(\Omega) \times L^2_0(\Omega)$, using (4.1) and (4.2) we can conclude that

$$\begin{aligned}\mathcal{A}_h(\boldsymbol{u} - \boldsymbol{u}_h^c, p - p_h; \boldsymbol{v}, q) &= \int_\Omega \boldsymbol{f}\cdot\boldsymbol{v} d\boldsymbol{x} - \tilde{A}_h(\boldsymbol{u}_h^c, \boldsymbol{v}) - B_h(p_h, \boldsymbol{v}) - B_h(q, \boldsymbol{u}_h^c) \\ &= \int_\Omega \boldsymbol{f}\cdot\boldsymbol{v} d\boldsymbol{x} - D_h(\boldsymbol{u}_h^c, \boldsymbol{v}) - J_h(\boldsymbol{u}_h^c, \boldsymbol{v}) - O_h(\boldsymbol{u}_h^c, \boldsymbol{v}) \\ &\quad - B_h(p_h, \boldsymbol{v}) - B_h(q, \boldsymbol{u}_h^c) \\ &= \int_\Omega \boldsymbol{f}\cdot\boldsymbol{v} d\boldsymbol{x} - \tilde{A}_h(\boldsymbol{u}_h, \boldsymbol{v}) + D_h(\boldsymbol{u}_h^r, \boldsymbol{v}) + J_h(\boldsymbol{u}_h^r, \boldsymbol{v}) \\ &\quad + O_h(\boldsymbol{u}_h^r, \boldsymbol{v}) - B_h(p_h, \boldsymbol{v}) + B_h(q, \boldsymbol{u}_h^r).\end{aligned} \tag{4.17}$$

From (2.5) and (4.2), it follows that

$$\begin{aligned}0 = -\int_\Omega \boldsymbol{f}\cdot\boldsymbol{I}_h\boldsymbol{v} d\boldsymbol{x} + \mathcal{A}_h(\boldsymbol{u}_h, p_h; \boldsymbol{I}_h\boldsymbol{v}, 0) &= -\int_\Omega \boldsymbol{f}\cdot\boldsymbol{I}_h\boldsymbol{v} d\boldsymbol{x} + \tilde{A}_h(\boldsymbol{u}_h, \boldsymbol{I}_h\boldsymbol{v}) \\ &\quad + \mathcal{K}_h(\boldsymbol{u}_h, \boldsymbol{I}_h\boldsymbol{v}) + B_h(p_h, \boldsymbol{I}_h\boldsymbol{v}),\end{aligned} \tag{4.18}$$

where $\boldsymbol{I}_h$ is the interpolant defined in Lemma 4.7.

Adding (4.17) and (4.18) and decomposing into three parts, we have

$$\mathcal{A}_h(\boldsymbol{u}-\boldsymbol{u}_h^c, p-p_h; \boldsymbol{v}, q) = T_1 + T_2 + T_3, \tag{4.19}$$

where

$$\begin{aligned} T_1 &= \int_\Omega \boldsymbol{f}\cdot(\boldsymbol{v}-\boldsymbol{I}_h\boldsymbol{v})d\boldsymbol{x} - \tilde{A}_h(\boldsymbol{u}_h, \boldsymbol{v}-\boldsymbol{I}_h\boldsymbol{v}) - B_h(p_h, \boldsymbol{v}-\boldsymbol{I}_h\boldsymbol{v}),\\ T_2 &= D_h(\boldsymbol{u}_h^r, \boldsymbol{v}) + J_h(\boldsymbol{u}_h^r, \boldsymbol{v}) + O_h(\boldsymbol{u}_h^r, \boldsymbol{v}) + B_h(q, \boldsymbol{u}_h^r),\\ T_3 &= \mathcal{K}_h(\boldsymbol{u}_h, \boldsymbol{I}_h\boldsymbol{v}). \end{aligned}$$

The result in Lemma 4.9 implies

$$T_1 \lesssim (\eta + \boldsymbol{\Theta})|||\boldsymbol{v}|||. \tag{4.20}$$

Applying the continuity results from Lemma 4.1 in the first three terms of T_2 and the Cauchy–Schwarz inequality in the last term of T_2, and then using Lemma 4.8, gives

$$T_2 \lesssim \eta|||(\boldsymbol{v}, q)|||. \tag{4.21}$$

The estimate in Lemma 4.2 leads to

$$T_3 \lesssim \gamma^{-1/2}\Big(\sum_{K\in\mathcal{T}_h}\eta_{J_K}^2\Big)^{1/2}|||\boldsymbol{v}|||. \tag{4.22}$$

Combining (4.16), (4.19), (4.20), (4.21), and (4.22) leads to the stated result. ∎

The reliability bound in Theorem 3.2 follows from a combination of (4.12), Lemma 4.8, and Lemma 4.10.

4.4. Proof of Theorem 3.3. In this subsection, we prove the efficiency bound for η_{R_K}, η_{J_K}, and η_{E_K}. The bubble function technique as given in [19, 22, 14] is used to prove the theorem.

LEMMA 4.11. *Let K be the element of $\mathcal{T}_h$. Let χ_K denote the standard bubble polynomial function on K. Then the following estimates hold:*

$$||\chi_K\boldsymbol{v}||_{0,K} \lesssim ||\boldsymbol{v}||_{0,K}, \tag{4.23}$$

$$||\boldsymbol{v}||_{0,K} \lesssim ||\chi_K^{1/2}\boldsymbol{v}||_{0,K}, \tag{4.24}$$

$$||\nabla(\chi_K\boldsymbol{v})||_{0,K} \lesssim h_K^{-1}||\boldsymbol{v}||_{0,K}, \tag{4.25}$$

$$||\chi_K\boldsymbol{v}||_{L^\infty(K)} \lesssim h_K^{-1}||\boldsymbol{v}||_{0,K}, \tag{4.26}$$

where $\boldsymbol{v}$ denotes a vector valued polynomial function on K.

Proof. The estimates (4.23) and (4.24) follow from Lemma 4.1 of [19]. The estimates (4.25) and (4.26) follow from (4.9) and (4.10) of [14]. ∎

4.4.1. Lower bound for the trace residual $\boldsymbol{\eta_{J_K}}$. The efficiency bound for the trace residual η_{J_K} is given in the following lemma.

LEMMA 4.12. *There holds*

$$\Big(\sum_{K\in\mathcal{T}_h}\eta_{J_K}^2\Big)^{1/2} \lesssim |||\boldsymbol{u}-\boldsymbol{u}_h||| + |\boldsymbol{u}-\boldsymbol{u}_h|_A + \nu^{-1/2}||p-p_h||_{\mathcal{T}_h}.$$

Proof. Noting that $[\![\boldsymbol{u}]\!]|_E = 0$ for $\boldsymbol{u} \in \boldsymbol{H}_0^1(\Omega)$, it follows that

$$\begin{aligned}\eta_{J_K}^2 :&= \frac{1}{2}\sum_{E\in\partial K\setminus\Gamma}\left(\frac{\gamma\nu}{h_E}+\beta h_E+\frac{h_E}{\nu}\right)||[\![\boldsymbol{u}_h]\!]||_{0,E}^2+\sum_{E\in\partial K\cap\Gamma}\left(\frac{\gamma\nu}{h_E}+\beta h_E+\frac{h_E}{\nu}\right)||\boldsymbol{u}_h||_{0,E}^2\\ &= \frac{1}{2}\sum_{E\in\partial K\setminus\Gamma}\left(\frac{\gamma\nu}{h_E}+\beta h_E+\frac{h_E}{\nu}\right)||[\![\boldsymbol{u}_h]\!]-[\![\boldsymbol{u}]\!]||_{0,E}^2\\ &+\sum_{E\in\partial K\cap\Gamma}\left(\frac{\gamma\nu}{h_E}+\beta h_E+\frac{h_E}{\nu}\right)||\boldsymbol{u}_h-\boldsymbol{u}||_{0,E}^2.\end{aligned}$$

Moreover, we have

$$\Big(\sum_{K\in\mathcal{T}_h}\eta_{J_K}^2\Big)^{1/2}\lesssim |||\boldsymbol{u}-\boldsymbol{u}_h|||+|\boldsymbol{u}-\boldsymbol{u}_h|_A+\nu^{-1/2}||p-p_h||_{\mathcal{T}_h}. \qquad \square$$

4.4.2. Lower bound for the internal residual $\boldsymbol{\eta_{R_K}}$. In the next lemma, we establish the efficiency bound for the internal residual η_{R_K}.

LEMMA 4.13. *There holds*

$$\Big(\sum_{K\in\mathcal{T}_h}\eta_{R_K}^2\Big)^{1/2}\lesssim |||\boldsymbol{u}-\boldsymbol{u}_h|||+|\boldsymbol{u}-\boldsymbol{u}_h|_A+\nu^{-1/2}||p-p_h||_{\mathcal{T}_h}+\boldsymbol{\Theta}.$$

Proof. For each element $K\in\mathcal{T}_h$, we define

$$R|_K=(\boldsymbol{f}_h+\nu\Delta\boldsymbol{u}_h-\underline{\boldsymbol{a}}_h\cdot\nabla\boldsymbol{u}_h-b_h\boldsymbol{u}_h-\nabla p_h)|_K.$$

Next, we set $W|_K=\rho_K^2 R\chi_K$. Using Lemma 4.11 gives

$$\begin{aligned}\sum_{K\in\mathcal{T}_h}\eta_{R_K}^2 &= \sum_{K\in\mathcal{T}_h}\rho_K^2||R||_{0,K}^2\lesssim (R,\rho_K^2\chi_K R)_{\mathcal{T}_h}\\ &= (R,W)_{\mathcal{T}_h}=(\boldsymbol{f}_h+\nu\Delta\boldsymbol{u}_h-\underline{\boldsymbol{a}}_h\cdot\nabla\boldsymbol{u}_h-b_h\boldsymbol{u}_h-\nabla p_h,W)_{\mathcal{T}_h}.\end{aligned}$$

Noting that $(\boldsymbol{f}+\nu\Delta\boldsymbol{u}-\underline{\boldsymbol{a}}\cdot\nabla\boldsymbol{u}-b\boldsymbol{u}-\nabla p)|_K=0$ for the exact solution $(\boldsymbol{u},p)$, we first subtract, then integrate by parts and note that $W|_{\partial K}=0$, to give

$$\begin{aligned}\sum_{K\in\mathcal{T}_h}\eta_{R_K}^2\lesssim&(\nu(\nabla(\boldsymbol{u}-\boldsymbol{u}_h),\nabla W)_{\mathcal{T}_h}-((\boldsymbol{u}-\boldsymbol{u}_h)\underline{\boldsymbol{a}}^T,\nabla W)_{\mathcal{T}_h}+((b-\nabla\cdot\underline{\boldsymbol{a}})(\boldsymbol{u}-\boldsymbol{u}_h),W)_{\mathcal{T}_h}\\ &+(p_h-p,\nabla\cdot W)_{\mathcal{T}_h})+((\boldsymbol{f}_h-\boldsymbol{f})+(\underline{\boldsymbol{a}}-\underline{\boldsymbol{a}}_h)\cdot\nabla\boldsymbol{u}_h+(b-b_h)\boldsymbol{u}_h,W)_{\mathcal{T}_h}.\end{aligned}$$

Applying the Cauchy–Schwarz inequality implies

$$\begin{aligned}\sum_{K\in\mathcal{T}_h}\eta_{R_K}^2\lesssim&\Big(|||\boldsymbol{u}-\boldsymbol{u}_h|||+|\boldsymbol{u}-\boldsymbol{u}_h|_A+\nu^{-1/2}||p-p_h||_{\mathcal{T}_h}+\boldsymbol{\Theta}\Big)\\ &\times\Big(|||W|||^2+\rho_K^{-2}||W||_{\mathcal{T}_h}^2\Big)^{1/2}.\end{aligned}$$

Using Lemma 4.11, it follows that

$$\sum_{K\in\mathcal{T}_h}\eta_{R_K}^2\lesssim(|||\boldsymbol{u}-\boldsymbol{u}_h|||+|\boldsymbol{u}-\boldsymbol{u}_h|_A+\nu^{-1/2}||p-p_h||_{\mathcal{T}_h}+\boldsymbol{\Theta})\Big(\sum_{K\in\mathcal{T}_h}\eta_{R_K}^2\Big)^{1/2}.$$

This completes the proof. $\square$

4.4.3. Lower bound for the edge residual $\boldsymbol{\eta_{E_K}}$. Let E denote an interior edge shared by two elements K and K'. Now we define the standard polynomial bubble function χ_E on E. Next, we assume $\delta_E = \{K, K'\}$. In the case of regular edge E, we choose $\widetilde{K} = K'$. If one vertex of E is a hanging node, we may choose E as an entire edge of K. Moreover, we denote by $\widetilde{K} \subset K'$ the largest rectangle contained in K'. Therefore E is also one of the entire edges of $\widetilde{K}$. Now we assume $\widetilde{\delta}_E = \{K, \widetilde{K}\}$. While $\boldsymbol{\sigma}$ is a vector valued polynomial function on E, it follows that

$$||\boldsymbol{\sigma}||_{0,E} \lesssim ||\chi_E^{1/2}\boldsymbol{\sigma}||_{0,E}.$$

Moreover we can define an extension $\boldsymbol{\sigma}_\chi \in \boldsymbol{H}_0^1(K \cap \widetilde{K})$ such that $\boldsymbol{\sigma}_\chi|_E = \chi_E\boldsymbol{\sigma}$. From [19, 1, 14], we have

$$||\boldsymbol{\sigma}_\chi||_{0,K} \lesssim h_E^{1/2}||\boldsymbol{\sigma}||_{0,E} \quad \forall K \in \widetilde{\delta}_E, \tag{4.27}$$

$$||\nabla\boldsymbol{\sigma}_\chi||_{0,K} \lesssim h_E^{-1/2}||\boldsymbol{\sigma}||_{0,E} \quad \forall K \in \widetilde{\delta}_E, \tag{4.28}$$

$$||\boldsymbol{\sigma}_\chi||_{\boldsymbol{L}^\infty(K)} \lesssim h_E^{-1/2}||\boldsymbol{\sigma}||_{0,E} \quad \forall K \in \widetilde{\delta}_E. \tag{4.29}$$

LEMMA 4.14. *There holds*

$$\Big(\sum_{K\in\mathcal{T}_h} \eta_{E_K}^2\Big)^{1/2} \lesssim |||\boldsymbol{u} - \boldsymbol{u}_h||| + |\boldsymbol{u} - \boldsymbol{u}_h|_A + \nu^{-1/2}||p - p_h||_{\mathcal{T}_h} + \boldsymbol{\Theta}.$$

Proof. Define

$$\Lambda = \sum_{E\in\mathcal{E}_I(\mathcal{T}_h)} \nu^{-1/2}\rho_E[\![p_h\underline{I} - \nu\nabla\boldsymbol{u}_h]\!]\chi_E.$$

Note that the solution $(\boldsymbol{u}, p)$ of the Oseen problem satisfies

$$[\![p\underline{I} - \nu\nabla\boldsymbol{u}]\!]|_E = 0.$$

Then, we have

$$\sum_{K\in\mathcal{T}_h} \eta_{E_K}^2 \lesssim \sum_{E\in\mathcal{E}^i(\mathcal{T}_h)} ([\![p_h\underline{I} - \nu\nabla\boldsymbol{u}_h]\!], \Lambda)_E = \sum_{E\in\mathcal{E}^i(\mathcal{T}_h)} ([\![p_h\underline{I} - \nu\nabla\boldsymbol{u}_h]\!] - [\![p\underline{I} - \nu\nabla\boldsymbol{u}]\!], \Lambda)_E.$$

Applying the Green's formula over each of the two elements of $\tilde{\delta}_E$ implies

$$\begin{aligned}
&\sum_{E\in\mathcal{E}^i(\mathcal{T}_h)} ([\![p_h\underline{I} - \nu\nabla\boldsymbol{u}_h]\!] - [\![p\underline{I} - \nu\nabla\boldsymbol{u}]\!], \Lambda)_E \\
&\quad= \sum_{E\in\mathcal{E}^i(\mathcal{T}_h)} \sum_{K\in\widetilde{\delta}_E} \Big(\int_K (-\nu\Delta(\boldsymbol{u} - \boldsymbol{u}_h) + \nabla(p - p_h))\Lambda d\boldsymbol{x} \\
&\qquad + \int_K (-\nu\nabla(\boldsymbol{u} - \boldsymbol{u}_h) + (p - p_h)\underline{I}) : \nabla\Lambda d\boldsymbol{x} \Big).
\end{aligned}$$

Using the fact that $(\boldsymbol{u}, p)$ solves the Oseen problem gives

$$\begin{aligned}\sum_{K\in\mathcal{T}_h}\eta_{E_K}^2 \lesssim & \sum_{E\in\mathcal{E}^i(\mathcal{T}_h)}\sum_{K\in\widetilde{\delta}_E}\int_K(\boldsymbol{f}_h+\nu\Delta\boldsymbol{u}_h-\underline{\boldsymbol{a}}_h\cdot\nabla\boldsymbol{u}_h-b_h\boldsymbol{u}_h-\nabla p_h)\cdot\Lambda d\boldsymbol{x}\\ &+\sum_{E\in\mathcal{E}^i(\mathcal{T}_h)}\sum_{K\in\widetilde{\delta}_E}\int_K((\boldsymbol{f}-\boldsymbol{f}_h)+(\underline{\boldsymbol{a}}_h-\underline{\boldsymbol{a}})\cdot\nabla\boldsymbol{u}_h+(b-b_h)\boldsymbol{u}_h)\cdot\Lambda d\boldsymbol{x}\\ &+\sum_{E\in\mathcal{E}^i(\mathcal{T}_h)}\sum_{K\in\widetilde{\delta}_E}\int_K(\underline{\boldsymbol{a}}\cdot\nabla(\boldsymbol{u}_h-\boldsymbol{u})+b(\boldsymbol{u}_h-\boldsymbol{u}))\cdot\Lambda d\boldsymbol{x}\\ &+\sum_{E\in\mathcal{E}^i(\mathcal{T}_h)}\sum_{K\in\widetilde{\delta}_E}\int_K(-\nu\nabla(\boldsymbol{u}-\boldsymbol{u}_h)+(p-p_h)\underline{I}):\nabla\Lambda d\boldsymbol{x}\\ &\lesssim T_1+T_2+T_3+T_4.\end{aligned}$$

Using the Cauchy–Schwarz inequality, the shape-regularity of the mesh, Lemma 4.13, and $||\cdot||_{0,\widetilde{K}}\lesssim||\cdot||_{0,K'}$ leads to

$$T_1\lesssim(|||\boldsymbol{u}-\boldsymbol{u}_h|||+\nu^{-1/2}||p-p_h||_{\mathcal{T}_h}+\boldsymbol{\Theta})\Big(\sum_{E\in\mathcal{E}^i(\mathcal{T}_h)}\sum_{K\in\widetilde{\delta}_E}\rho_E^{-2}||\Lambda||_{0,K}^2\Big)^{1/2}.$$

From (4.27), we have

$$\Big(\sum_{E\in\mathcal{E}^i(\mathcal{T}_h)}\sum_{K\in\widetilde{\delta}_E}\rho_E^{-2}||\Lambda||_{0,K}^2\Big)^{1/2}\lesssim\Big(\sum_{K\in\mathcal{T}_h}\eta_{E_K}^2\Big)^{1/2}.$$

Hence, the following estimate holds:

$$T_1\lesssim(|||\boldsymbol{u}-\boldsymbol{u}_h|||+|\boldsymbol{u}-\boldsymbol{u}_h|_A+\nu^{-1/2}||p-p_h||_{\mathcal{T}_h}+\boldsymbol{\Theta})\Big(\sum_{K\in\mathcal{T}_h}\eta_{E_K}^2\Big)^{1/2}.$$

Applying the Cauchy–Schwarz inequality, the shape-regularity of the mesh, $||\cdot||_{0,\widetilde{K}}\lesssim||\cdot||_{0,K'}$, and (4.27) in T_2 implies

$$T_2\lesssim\boldsymbol{\Theta}\Big(\sum_{K\in\mathcal{T}_h}\eta_{E_K}^2\Big)^{1/2}.$$

Using integration by parts in T_3 yields

$$\begin{aligned}T_3=&\sum_{E\in\mathcal{E}^i(\mathcal{T}_h)}\sum_{K\in\widetilde{\delta}_E}\int_K(-\nabla\cdot\underline{\boldsymbol{a}}+b)(\boldsymbol{u}_h-\boldsymbol{u})\cdot\Lambda d\boldsymbol{x}+\sum_{E\in\mathcal{E}^i(\mathcal{T}_h)}\int_E(\underline{\boldsymbol{a}}\cdot[\![\boldsymbol{u_h}]\!])\cdot\Lambda ds\\ &-\sum_{E\in\mathcal{E}^i(\mathcal{T}_h)}\sum_{K\in\widetilde{\delta}_E}\int_K(\boldsymbol{u}_h-\boldsymbol{u})\underline{\boldsymbol{a}}^T:\nabla\Lambda d\boldsymbol{x}.\end{aligned}$$

Using the Cauchy–Schwarz inequality, the shape-regularity of the mesh, $||\cdot||_{0,\widetilde{K}}\lesssim||\cdot||_{0,K'}$, and (4.28) leads to

$$T_3\lesssim|||\boldsymbol{u}-\boldsymbol{u}_h|||\Big(\sum_{K\in\mathcal{T}_h}\eta_{E_K}^2\Big)^{1/2}+|\boldsymbol{u}-\boldsymbol{u}_h|_A\Big(\sum_{K\in\mathcal{T}_h}\eta_{E_K}^2\Big)^{1/2}.$$

By using the Cauchy–Schwarz inequality, the shape-regularity of the mesh, $||\cdot||_{0,\widetilde{K}} \lesssim ||\cdot||_{0,K'}$, and (4.28) in T_4, we obtain that

$$T_4 \lesssim (|||\boldsymbol{u}-\boldsymbol{u}_h||| + \nu^{-1/2}||p-p_h||_{\mathcal{T}_h})\Big(\sum_{K\in\mathcal{T}_h}\eta_{E_K}^2\Big)^{1/2}.$$

Combining the above estimates T_1, T_2, T_3, and T_4 implies the stated result. ∎

The efficiency bound in Theorem 3.3 follows from a combination of Lemmas 4.12, 4.13, and 4.14.

Remark 4.1. In section 5, we provide numerical evidence that the convergence rate of $|\boldsymbol{u}-\boldsymbol{u}_h|_A$ is at least of the same order as the error $|||e||| = |||(\boldsymbol{u}-\boldsymbol{u}_h, p-p_h)|||$ and even of higher order. Assume that the error $|||e|||$ converges with optimal order $\mathcal{O}(N^{-k/2})$, where N and k are the number of degrees of freedom (DOF) and the polynomial order of $RT_k \times Q_k$, respectively. Then from (4.14), we have

$$|(\boldsymbol{u}-\boldsymbol{u}_h)\underline{\boldsymbol{a}}^T|_\star \lesssim \nu^{-1/2}||\boldsymbol{u}-\boldsymbol{u}_h||_0.$$

Assume that $||\boldsymbol{u}-\boldsymbol{u}_h||_0$ converges with optimal order $\mathcal{O}(N^{-k/2-1/2})$; then

$$|(\boldsymbol{u}-\boldsymbol{u}_h)\underline{\boldsymbol{a}}^T|_\star \lesssim (N^{-1/2}\nu^{-1})\,\nu^{1/2}N^{-k/2}.$$

Here $N^{-1/2}\nu^{-1}$ is the local mesh Reynolds number. Thus, the convergence rate of $|(\boldsymbol{u}-\boldsymbol{u}_h)\underline{\boldsymbol{a}}^T|_\star$ is at least of the same order as the error $|||e|||$. Similarly, we have

$$\Big(\sum_{E\in\mathcal{E}(\mathcal{T}_h)} h_E\nu^{-1}||[\![\boldsymbol{u}-\boldsymbol{u}_h]\!]||_{0,E}^2\Big)^{1/2} \lesssim (N^{-1/2}\nu^{-1})\,\nu^{1/2}N^{-k/2},$$

$$\Big(\sum_{E\in\mathcal{E}(\mathcal{T}_h)} h_E\beta||[\![\boldsymbol{u}-\boldsymbol{u}_h]\!]||_{0,E}^2\Big)^{1/2} \lesssim \beta^{1/2}\,N^{-k/2-1/2}.$$

Hence the conclusion for $|(\boldsymbol{u}-\boldsymbol{u}_h)\underline{\boldsymbol{a}}^T|_\star$ can also hold for the error $|\boldsymbol{u}-\boldsymbol{u}_h|_A$.

5. Numerical results. In this section, we show the practical applicability of the proposed numerical schemes to validate the theoretical results obtained for the Oseen problem in two dimensions. Moreover, we discuss the convergence behavior for uniform and adaptive meshes using an a posteriori error estimator. In particular, starting with an initial mesh $\mathcal{T}_0$, we use the iterative refinement loop

$$\text{Solve} \rightarrow \text{Estimate} \rightarrow \text{Mark} \rightarrow \text{Refine}$$

to construct the adaptively refined sequences of one-irregular rectangular meshes $\{\mathcal{T}_\ell\}$ with mesh size h_ℓ. For each $\mathcal{T}_\ell$ and associated $\boldsymbol{H}^{\text{div}}$-DG approximation, we compute $\eta_\ell^2 = \sum_{K\in\mathcal{T}_\ell}\eta_K^2$. Then, we construct a minimal set of marked rectangles $\mathcal{M}_\ell$ according to the bulk marking strategy [8], such that $\theta\eta_\ell^2 \le \eta_\ell^2(\mathcal{M}_\ell)$ for the bulk parameter $\theta = 1/2$. Mesh refinement is then done so that the resulting meshes are one-irregular. Let N_ℓ denotes the DOF such that

$$N_\ell := \dim(\boldsymbol{V}_h) + \dim(Q_h).$$

For uniform meshes, $\mathcal{O}(N_\ell^{-r}) \approx \mathcal{O}(h^{2r}),\ r > 0$.

Our implementation of the proposed method is based on the deal.II finite element library [2] and Amandus [13]. To solve the nonsymmetric linear saddle point system, we use the multigrid based solver, which is discussed in [18].

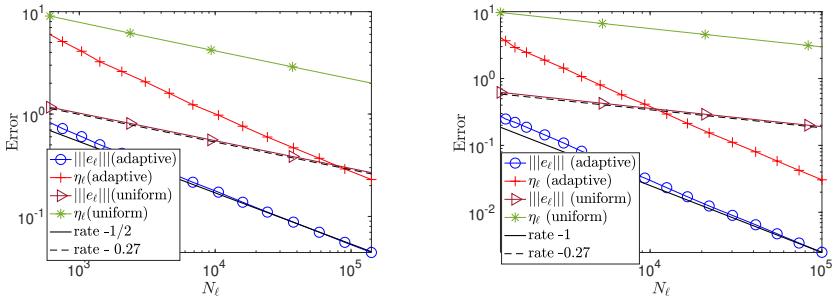

(a) (b)

FIG. 1. (a) $RT_1 \times Q_1$. (b) $RT_2 \times Q_2$.

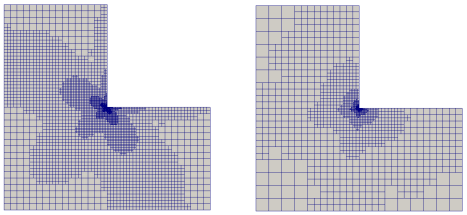

(a) (b)

FIG. 2. *Adaptive refined meshes for* (a) $RT_1 \times Q_1$ *(*58356 *DOF) and* (b) $RT_2 \times Q_2$ *(*54590 *DOF).*

5.1. L-shaped domain. This example is based on the standard singular solution of the Stokes problem with $\nu = 1$ and $\boldsymbol{f} = 0$ on an L-shaped domain $\Omega = (-1,1)^2 \setminus [0,1)^2$ with an inhomogeneous Dirichlet boundary condition (see [22, 10]). In polar coordinates, the exact velocity and pressure are

$$\boldsymbol{u} = r^\lambda \begin{pmatrix} (1+\lambda)\sin(\varphi)\Psi(\varphi) + \cos(\varphi)\Psi'(\varphi) \\ \sin(\varphi)\Psi'(\varphi) - (1+\lambda)\cos(\varphi)\Psi(\varphi) \end{pmatrix}, \quad p = -\frac{r^{\lambda-1}[(1+\lambda)^2\Psi'(\varphi) + \Psi'''(\varphi)]}{(1-\lambda)},$$

where

$$\Psi(\varphi) = \sin((1+\lambda)\varphi)\frac{\cos(\lambda\omega)}{1+\lambda} - \cos((1+\lambda)\varphi) - \sin((1-\lambda)\varphi)\frac{\cos(\lambda\omega)}{1-\lambda} + \cos((1-\lambda)\varphi),$$

with $\omega = 3\pi/2$ and $\lambda = 0.54448373678246$. At the re-entrant corner, the velocity and the pressure have singularities of the forms r^λ and $r^{\lambda-1}$, respectively. (The initial mesh $\mathcal{T}_0$ was generated with a uniform square mesh of 48 cells.) For $RT_1 \times Q_1$ and $RT_2 \times Q_2$ elements, the convergence results for uniform refinement meshes in Figures 1(a) and 1(b) show low-order convergence $\mathcal{O}(N_\ell^{-0.27})$ for the error $|||e_\ell|||$ and the proposed estimator η_ℓ. For uniform meshes, we cannot expect convergence orders better than λ in the energy norm $|||\cdot|||$. Moreover, the graph of the estimates η_ℓ is parallel to the error in energy norm $|||e_\ell|||$. Thus, this confirms that the error estimator is numerically reliable and efficient. In Figures 1(a) and 1(b), the convergence results based on adaptive refinement achieve the optimal convergence $\mathcal{O}(N_\ell^{-k/2})$, $k = 1, 2$, for the error $|||e_\ell|||$ and a posteriori error control η_ℓ. Figures 2(a) and 2(b) show the adaptivity refined meshes for $RT_k \times Q_k (k = 1, 2)$ elements. Moreover, Figures 2(a) and 2(b) show strong refinement toward the singularity.

5.2. Kovasznay's solution. In this example, we consider the two-dimensional analytical solution of the incompressible Navier–Stokes equations derived by Kovasznay in [15]. In the case of the Oseen problem, we choose the direction $\underline{\boldsymbol{a}} = \boldsymbol{u}$ and $b = 0$. Here, we present the results for $\nu = 1, 10^{-1}, 10^{-2}, 10^{-3}$, and 10^{-4}; see Figures 3, 4, and 5. (The initial mesh $\mathcal{T}_0$ was generated with a uniform square mesh of $256(16 \times 16)$ cells.) In Figure 3, the convergence results based on adaptive refinement achieve the optimal convergence $\mathcal{O}(N_\ell^{-1/2})$ for the error $|||e_\ell|||$ and a posteriori error control η_ℓ. The proposed a posteriori error control η_ℓ always overestimates the energy error $|||e_\ell|||$ because of agreement with the reliability result of Theorem 3.2. In Figure 3, we also plot the curve DERR that represents the error $\nu^{-1/2}||\boldsymbol{u} - \boldsymbol{u}_h||_{0,\Omega}$, which is the upper bound of $|(\boldsymbol{u} - \boldsymbol{u}_h)\underline{\boldsymbol{a}}^T|$ as shown in Remark 4.1. For $\nu = 1$, the curve DERR converges at a higher order than the energy error. For the smaller values of ν, the curve DERR decays with the same order as the energy error, but it becomes faster when interior and boundary layers are approximated well enough. The curve JERR represents the error $(\sum_{E\in\mathcal{E}(\mathcal{T}_h)}(\beta h_E + h_E\nu^{-1})|||[\![\boldsymbol{u}]\!]|||^2_{0,E})^{1/2}$. From Figure 3, we observe that the behaviors of the curves DERR and JERR are similar. From Figure 4, we observe that the ratio (effectivity index) of the estimator and the error $|||e_\ell|||$ is around 5.

5.3. Two-dimensional boundary layer. To conclude, we discuss a test problem that is also discussed in [3]. Here we choose $\Omega = (0,1)^2$, the direction $\underline{\boldsymbol{a}} = (1,1)$, and $b = 0$. The problem is constructed such that the exact solution is given by

$$\boldsymbol{u} = \mathrm{curl}\phi = \left(\frac{\partial\phi}{\partial y}, -\frac{\partial\phi}{\partial x}\right), \quad p = e^{x+y} - p_m,$$

where the potential function $\phi(x,y) = x^2y^2(1 - e^{\lambda(x-1)})^2(1 - e^{\lambda(y-1)})^2$ with $\lambda = 0.5/\sqrt{\nu}$ and $p_m \in \mathbb{R}$ is such that $\int_\Omega p = 0$. (The initial mesh $\mathcal{T}_0$ was generated with a uniform square mesh of 256 (16×16) cells.) In Figures 6(a) and 6(b), we show that the graph of a posteriori error control η_ℓ is parallel to the total error $e_{total}(|||e_\ell||| + JERR)$ for $\nu = 10^{-3}$ and $\nu = 10^{-4}$. Hence, this confirms that the proposed a posteriori error control η_ℓ is numerically reliable and efficient. In Figures 6(a) and 6(b), the convergence results based on adaptive refinement achieve the optimal convergence $\mathcal{O}(N_\ell^{-k/2})$, $k = 1, 2$, for the error $e_{total}(|||e_\ell||| + JERR)$ and a posteriori error control η_ℓ. Figures 8(a) and 8(b) show the adaptively refined meshes for $RT_k \times Q_k (k = 1, 2)$ elements. Moreover, Figures 8(a) and 8(b) show strong refinement toward the boundary layer. From Figures 7(a) and 7(b), we observe that the effectivity index of the estimator and the error e_{total} is around 5 for $k = 1$ and 8 for $k = 2$. From Figure 11 of [3], it is easily seen that the proposed estimator underestimates the true error for $\nu = 10^{-3}$. But our estimator always overestimates the energy error $|||e_\ell|||$ as well as the total error e_{total} because of agreement with the reliability result of Theorem 3.2. The computed velocity and pressure for $\nu = 10^{-3}$ are displayed in Figure 9.

Remark 5.1. In this article, we focused on an h-adaptive based a posteriori estimator. The effectivity index deteriorates when we use $RT_2\times Q_2$ instead of $RT_1\times Q_1$. It may be possible to overcome this variation by using an hp-adaptive based a posteriori estimator.

Remark 5.2. In the examples in subsections 5.2 and 5.3, we used the same initial mesh $\mathcal{T}_0$ for different Reynolds numbers. Specifically, the initial mesh $\mathcal{T}_0$ was generated with a uniform square mesh of 256 (16×16) cells. Note that ν^{-1} represents the Reynolds number. Moreover, $h\nu^{-1}$ represents the local mesh Reynolds number. So it may be possible to choose different refinement levels for different Reynolds numbers.

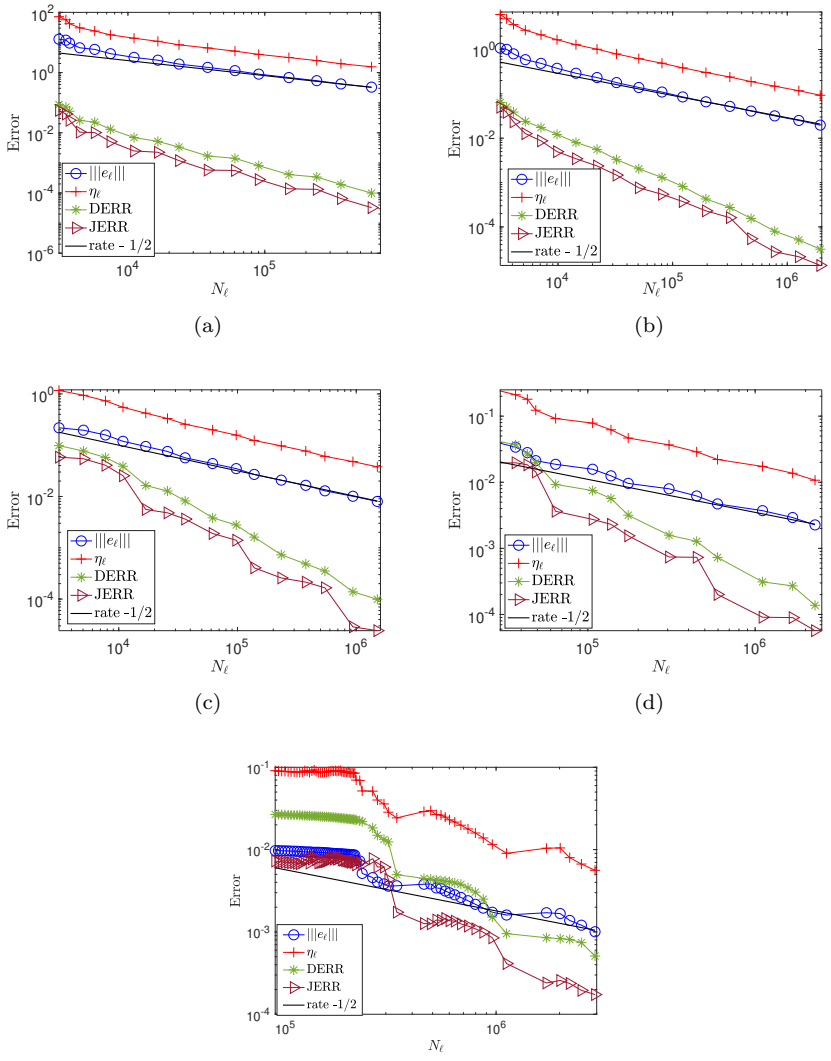

FIG. 3. *Convergence behavior for* (a) $\nu = 1$, (b) $\nu = 10^{-1}$, (c) $\nu = 10^{-2}$, (d) $\nu = 10^{-3}$, *and* (e) $\nu = 10^{-4}$ *with* $RT_1 \times Q_1$.

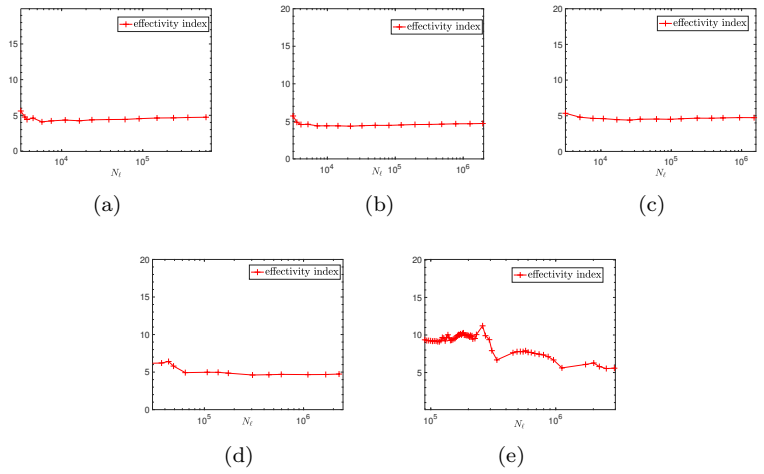

FIG. 4. *Effectivity index for* (a) $\nu = 1$, (b) $\nu = 10^{-1}$, (c) $\nu = 10^{-2}$, (d) $\nu = 10^{-3}$, *and* (e) $\nu = 10^{-4}$ *with* $RT_1 \times Q_1$.

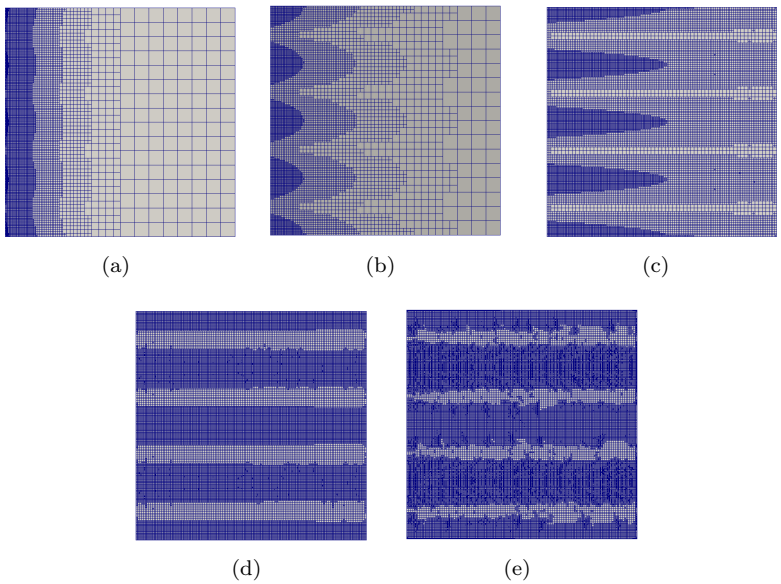

FIG. 5. *Adaptive refined meshes for* (a) $\nu = 1$ *(149990 DOF),* (b) $\nu = 10^{-1}$ *(119222 DOF),* (c) $\nu = 10^{-2}$ *(297786 DOF),* (d) $\nu = 10^{-3}$ *(610766 DOF), and* (e) $\nu = 10^{-4}$ *(959896 DOF) with* $RT_1 \times Q_1$.

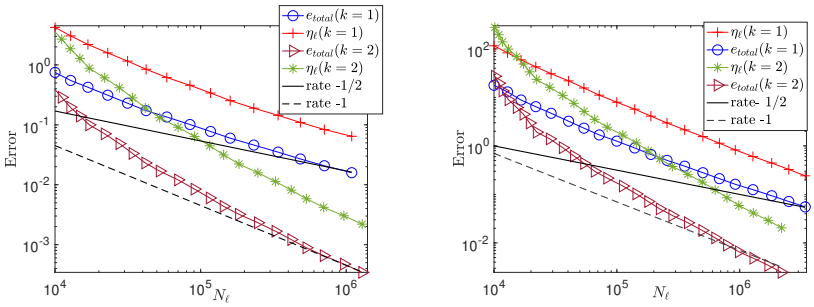

FIG. 6. *Convergence behavior for* (a) $\nu = 10^{-3}$, (b) $\nu = 10^{-4}$.

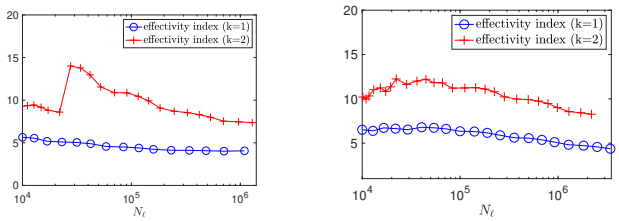

FIG. 7. *Effectivity index for* (a) $\nu = 10^{-3}$ *and* (b) 10^{-4}.

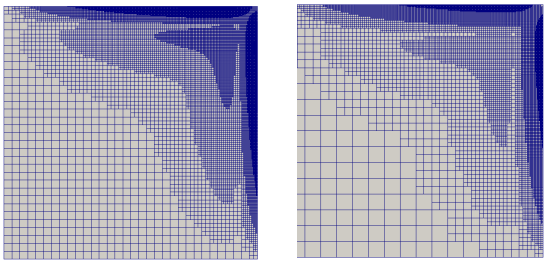

FIG. 8. *Adaptive refined meshes for* (a) $RT_1 \times Q_1$ *(340312 DOF) and* (b) $RT_2 \times Q_2$ *(419280 DOF) with* $\nu = 10^{-3}$.

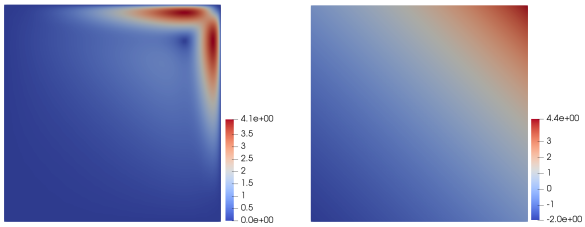

(a) (b)

FIG. 9. *Plots of* (a) *discrete velocity and* (b) *discrete pressure for* $RT_1 \times Q_1$ *(*115016 *DOF) with* $\nu = 10^{-3}$.

6. Conclusions. In this paper, we have presented a robust a posteriori error estimator for divergence-conforming DG methods of the Oseen equation. Upper and local lower bounds for the velocity-pressure error in terms of the energy norm and a seminorm associated with the convective term in the equation are derived. Moreover, we also proved that the ratio (effectivity index) of upper and lower bounds is independent of the Reynolds number of the problem. Thus the proposed estimator is fully robust. Specific numerical experiments demonstrated the effectiveness of the a posteriori error estimator for a wide range of Reynolds numbers. Establishing robustness in the error estimation process is fundamentally important when solving flow problems with high Reynolds numbers.

Finally, we mention that our proposed theory is also applicable to exactly divergence-free BDM_k/P_{k-1} elements on regular triangular meshes; see [7].

Acknowledgments. We are grateful to Dr. Noman Shakir for his suggestions in coding and we thank two anonymous referees and Dr. Hina Vasishtha for very useful comments.

REFERENCES

[1] M. AINSWORTH AND J T. ODEN, *A Posteriori Error Estimation in Finite Element Analysis*, Pure Appl. Math. (N. Y.) 37, John Wiley & Sons, 2000.

[2] W. BANGERTH, T. HEISTER, L. HELTAI, G. KANSCHAT, M. KRONBICHLER, M. MAIER, AND B. TURCKSIN, *The deal.*II *library, version* 8.3, Arch. Numer. Software, 4 (2016), pp. 1–11.

[3] T. P. BARRIOS, J. M. CASCÓN, AND M. GONZÁLEZ, *Augmented mixed finite element method for the Oseen problem: A priori and a posteriori error analyses*, Comput. Methods Appl. Mech. Engrg., 313 (2017), pp. 216–238, https://doi.org/10.1016/j.cma.2016.09.012.

[4] F. BREZZI AND M. FORTIN, *Mixed and Hybrid Finite Element Methods*, Springer Ser. Comput. Math. 15, Springer-Verlag, 1991.

[5] B. COCKBURN, G. KANSCHAT, AND D. SCHÖTZAU, *The local discontinuous Galerkin method for the Oseen equations*, Math. Comp., 73 (2004), pp. 569–593, https://doi.org/10.1090/S0025-5718-03-01552-7.

[6] B. COCKBURN, G. KANSCHAT, AND D. SCHÖTZAU, *A locally conservative LDG method for the incompressible Navier-Stokes equations*, Math. Comp., 74 (2005), pp. 1067–1095, https://doi.org/10.1090/S0025-5718-04-01718-1.

[7] B. COCKBURN, G. KANSCHAT, AND D. SCHÖTZAU, *A note on discontinuous Galerkin divergence-free solutions of the Navier–Stokes equations*, J. Sci. Comput., 31 (2007), pp. 61–73, https://doi.org/10.1007/s10915-006-9107-7.

[8] W. DÖRFLER, *A convergent adaptive algorithm for Poisson's equation*, SIAM J. Numer. Anal., 33 (1996), pp. 1106–1124, https://doi.org/10.1137/0733054.

[9] V. GIRAULT AND P.-A. RAVIART, *Finite Element Methods for Navier-Stokes Equations: Theory and Algorithms*, Springer Ser. Comput. Math. 5, Springer-Verlag, 1986.

[10] P. Houston, D. Schötzau, and T. P. Wihler, *Energy norm shape a posteriori error estimation for mixed discontinuous Galerkin approximations of the Stokes problem*, J. Sci. Comput., 22 (2005), pp. 347–370, https://doi.org/10.1007/s10915-004-4143-7.
[11] P. Houston, D. Schötzau, and T. P. Wihler, *Energy norm a posteriori error estimation of hp-adaptive discontinuous Galerkin methods for elliptic problems*, Math. Models Methods Appl. Sci., 17 (2007), pp. 33–62, https://doi.org/10.1142/S0218202507001826.
[12] P. Houston, E. Süli, and T. P. Wihler, *A posteriori error analysis of hp-version discontinuous Galerkin finite-element methods for second-order quasi-linear elliptic PDEs*, IMA J. Numer. Anal., 28 (2008), pp. 245–273, https://doi.org/10.1093/imanum/drm009.
[13] G. Kanschat, *Amandus Software*, https://bitbucket.org/guidokanschat/amandus.
[14] G. Kanschat and D. Schötzau, *Energy norm a posteriori error estimation for divergence-free discontinuous Galerkin approximations of the Navier–Stokes equations*, Int. J. Numer. Methods Fluids, 57 (2008), pp. 1093–1113, https://doi.org/10.1002/fld.1795.
[15] L. I. G. Kovasznay, *Laminar flow behind a two-dimensional grid*, Math. Proc. Cambridge Philos. Soc., 44 (1948), pp. 58–62, https://doi.org/10.1017/S0305004100023999.
[16] D. Schötzau, C. Schwab, and A. Toselli, *Mixed hp-DGFEM for incompressible flows*, SIAM J. Numer. Anal., 40 (2002), pp. 2171–2194, https://doi.org/10.1137/S0036142901399124.
[17] D. Schötzau and L. Zhu, *A robust a-posteriori error estimator for discontinuous Galerkin methods for convection–diffusion equations*, Appl. Numer. Math., 59 (2009), pp. 2236–2255, https://doi.org/10.1016/j.apnum.2008.12.014.
[18] N. Shakir, *Multilevel Schwarz Methods for Incompressible Flow Problems*, Ph.D. thesis, Heidelberg University, 2017.
[19] R. Verfürth, *A posteriori error estimation and adaptive mesh-refinement techniques*, J. Comput. Appl. Math., 50 (1994), pp. 67–83, https://doi.org/10.1016/0377-0427(94)90290-9.
[20] R. Verfürth, *Robust a posteriori error estimates for nonstationary convection-diffusion equations*, SIAM J. Numer. Anal., 43 (2005), pp. 1783–1802, https://doi.org/10.1137/040604273.
[21] R. Verfürth, *Robust a posteriori error estimates for stationary convection-diffusion equations*, SIAM J. Numer. Anal., 43 (2005), pp. 1766–1782, https://doi.org/10.1137/040604261.
[22] R. Verfürth, *A Posteriori Error Estimation Techniques for Finite Element Methods*, Oxford University Press, Oxford, 2013.
[23] L. Zhu and D. Schötzau, *A robust a posteriori error estimate for hp-adaptive DG methods for convection–diffusion equations*, IMA J. Numer. Anal., 31 (2010), pp. 971–1005, https://doi.org/10.1093/imanum/drp038.